Measurement of $D^{*\pm}$ production in deep inelastic scattering at HERA

ZEUS Collaboration

Abstract

The production of $D^{*\pm}$ mesons in deep inelastic ep scattering has been measured for exchanged photon virtualities $5 < Q^2 < 1000\,\mathrm{GeV}^2$, using an integrated luminosity of 363 pb^{-1} with the ZEUS detector at HERA. Differential cross sections have been measured and compared to next-to-leading-order QCD calculations. The cross-sections are used to extract the charm contribution to the proton structure functions, expressed in terms of the reduced charm cross section, $\sigma_{\mathrm{red}}^{c\bar{c}}$. Theoretical calculations based on fits to inclusive HERA data are compared to the results.

The ZEUS Collaboration

H. Abramowicz[45,aj], I. Abt[35], L. Adamczyk[13], M. Adamus[54], R. Aggarwal[7,c], S. Antonelli[4], P. Antonioli[3], A. Antonov[33], M. Arneodo[50], O. Arslan[5], V. Aushev[26,27,aa], Y. Aushev,[27,aa,ab], O. Bachynska[15], A. Bamberger[19], A.N. Barakbaev[25], G. Barbagli[17], G. Bari[3], F. Barreiro[30], N. Bartosik[15], D. Bartsch[5], M. Basile[4], O. Behnke[15], J. Behr[15], U. Behrens[15], L. Bellagamba[3], A. Bertolin[39], S. Bhadra[57], M. Bindi[4], C. Blohm[15], V. Bokhonov[26,aa], T. Bołd[13], E.G. Boos[25], K. Borras[15], D. Boscherini[3], D. Bot[15], I. Brock[5], E. Brownson[56], R. Brugnera[40], N. Brümmer[37], A. Bruni[3], G. Bruni[3], B. Brzozowska[53], P.J. Bussey[20], B. Bylsma[37], A. Caldwell[35], M. Capua[8], R. Carlin[40], C.D. Catterall[57], S. Chekanov[1], J. Chwastowski[12,e], J. Ciborowski[53,an], R. Ciesielski[15,h], L. Cifarelli[4], F. Cindolo[3], A. Contin[4], A.M. Cooper-Sarkar[38], N. Coppola[15,i], M. Corradi[3], F. Corriveau[31], M. Costa[49], G. D'Agostini[43], F. Dal Corso[39], J. del Peso[30], R.K. Dementiev[34], S. De Pasquale[4,a], M. Derrick[1], R.C.E. Devenish[38], D. Dobur[19,u], B.A. Dolgoshein[33,†], G. Dolinska[15], A.T. Doyle[20], V. Drugakov[16], L.S. Durkin[37], S. Dusini[39], Y. Eisenberg[55], P.F. Ermolov[34,†], A. Eskreys[12,†], S. Fang[15,j], S. Fazio[8], J. Ferrando[20], M.I. Ferrero[49], J. Figiel[12], B. Foster[38,af], G. Gach[13], A. Galas[12], E. Gallo[17], A. Garfagnini[40], A. Geiser[15], I. Gialas[21,x], A. Gizhko[15], L.K. Gladilin[34], D. Gladkov[33], C. Glasman[30], O. Gogota[27], Yu.A. Golubkov[34], P. Göttlicher[15,k], I. Grabowska-Bołd[13], J. Grebenyuk[15], I. Gregor[15], G. Grigorescu[36], G. Grzelak[53], O. Gueta[45], M. Guzik[13], C. Gwenlan[38,ag], T. Haas[15], W. Hain[15], R. Hamatsu[48], J.C. Hart[44], H. Hartmann[5], G. Hartner[57], E. Hilger[5], D. Hochman[55], R. Hori[47], A. Hüttmann[15], Z.A. Ibrahim[10], Y. Iga[42], R. Ingbir[45], M. Ishitsuka[46], A. Iudin[27,ac], H.-P. Jakob[5], F. Januschek[15], T.W. Jones[52], M. Jüngst[5], I. Kadenko[27], B. Kahle[15], S. Kananov[45], T. Kanno[46], U. Karshon[55], F. Karstens[19,v], I.I. Katkov[15,l], M. Kaur[7], P. Kaur[7,c], A. Keramidas[36], L.A. Khein[34], J.Y. Kim[9], D. Kisielewska[13], S. Kitamura[48,al], R. Klanner[22], U. Klein[15,m], E. Koffeman[36], N. Kondrashova[27,ad], O. Kononenko[27], P. Kooijman[36], Ie. Korol[15], I.A. Korzhavina[34], A. Kotański[14,f], U. Kötz[15], N. Kovalchuk[27,ae], H. Kowalski[15], O. Kuprash[15], M. Kuze[46], A. Lee[37], B.B. Levchenko[34], A. Levy[45], V. Libov[15], S. Limentani[40], T.Y. Ling[37], M. Lisovyi[15], E. Lobodzinska[15], W. Lohmann[16], B. Löhr[15], E. Lohrmann[22], K.R. Long[23], A. Longhin[39,ah], D. Lontkovskyi[15], O.Yu. Lukina[34], J. Maeda[46,ak], S. Magill[1], I. Makarenko[15], J. Malka[15], R. Mankel[15], A. Margotti[3], G. Marini[43], J.F. Martin[51], A. Mastroberardino[8], M.C.K. Mattingly[2], I.-A. Melzer-Pellmann[15], S. Mergelmeyer[5], S. Miglioranzi[15,n], F. Mohamad Idris[10], V. Monaco[49], A. Montanari[15], J.D. Morris[6,b], K. Mujkic[15,o], B. Musgrave[1], K. Nagano[24], T. Namsoo[15,p], R. Nania[3], A. Nigro[43], Y. Ning[11], T. Nobe[46], D. Notz[15], R.J. Nowak[53], A.E. Nuncio-Quiroz[5], B.Y. Oh[41], N. Okazaki[47], K. Olkiewicz[12], Yu. Onishchuk[27], K. Papageorgiu[21], A. Parenti[15], E. Paul[5], J.M. Pawlak[53], B. Pawlik[12], P. G. Pelfer[18], A. Pellegrino[36], W. Perlański[53,ao], H. Perrey[15], K. Piotrzkowski[29], P. Pluciński[54,ap], N.S. Pokrovskiy[25], A. Polini[3], A.S. Proskuryakov[34], M. Przybycień[13], A. Raval[15], D.D. Reeder[56], B. Reisert[35], Z. Ren[11], J. Repond[1], Y.D. Ri[48,am], A. Robertson[38], P. Roloff[15,n], I. Rubinsky[15], M. Ruspa[50], R. Sacchi[49], U. Samson[5], G. Sartorelli[4], A.A. Savin[56], D.H. Saxon[20], M. Schioppa[8], S. Schlenstedt[16], P. Schleper[22], W.B. Schmidke[35], U. Schneekloth[15], V. Schönberg[5], T. Schörner-Sadenius[15], J. Schwartz[31], F. Sciulli[11], L.M. Shcheglova[34], R. Shehzadi[5], S. Shimizu[47,n], I. Singh[7,c], I.O. Skillicorn[20], W. Słomiński[14,g], W.H. Smith[56], V. Sola[22], A. Solano[49], D. Son[28], V. Sosnovtsev[33], A. Spiridonov[15,q], H. Stadie[22], L. Stanco[39], N. Stefaniuk[27], A. Stern[45], T.P. Stewart[51], A. Stifutkin[33], P. Stopa[12], S. Suchkov[33], G. Susinno[8], L. Suszycki[13], J. Sztuk-

Dambietz[22], D. Szuba[22], J. Szuba[15,r], A.D. Tapper[23], E. Tassi[8,d], J. Terrón[30], T. Theedt[15], H. Tiecke[36], K. Tokushuku[24,y], J. Tomaszewska[15,s], A. Trofymov[27,ae], V. Trusov[27], T. Tsurugai[32], M. Turcato[22], O. Turkot[27,ae,t], T. Tymieniecka[54], M. Vázquez[36,n], A. Verbytskyi[15], O. Viazlo[27], N.N. Vlasov[19,w], R. Walczak[38], W.A.T. Wan Abdullah[10], J.J. Whitmore[41,ai], K. Wichmann[15,t], L. Wiggers[36], M. Wing[52], M. Wlasenko[5], G. Wolf[15], H. Wolfe[56], K. Wrona[15], A.G. Yagües-Molina[15], S. Yamada[24], Y. Yamazaki[24,z], R. Yoshida[1], C. Youngman[15], N. Zakharchuk[27,ae], A.F. Żarnecki[53], L. Zawiejski[12], O. Zenaiev[15], W. Zeuner[15,n], B.O. Zhautykov[25], N. Zhmak[26,aa], A. Zichichi[4], Z. Zolkapli[10], D.S. Zotkin[34]

II

1   *Argonne National Laboratory, Argonne, Illinois 60439-4815, USA* [A]
2   *Andrews University, Berrien Springs, Michigan 49104-0380, USA*
3   *INFN Bologna, Bologna, Italy* [B]
4   *University and INFN Bologna, Bologna, Italy* [B]
5   *Physikalisches Institut der Universität Bonn, Bonn, Germany* [C]
6   *H.H. Wills Physics Laboratory, University of Bristol, Bristol, United Kingdom* [D]
7   *Panjab University, Department of Physics, Chandigarh, India*
8   *Calabria University, Physics Department and INFN, Cosenza, Italy* [B]
9   *Institute for Universe and Elementary Particles, Chonnam National University, Kwangju, South Korea*
10 *Jabatan Fizik, Universiti Malaya, 50603 Kuala Lumpur, Malaysia* [E]
11 *Nevis Laboratories, Columbia University, Irvington on Hudson, New York 10027, USA* [F]
12 *The Henryk Niewodniczanski Institute of Nuclear Physics, Polish Academy of Sciences, Krakow, Poland* [G]
13 *AGH-University of Science and Technology, Faculty of Physics and Applied Computer Science, Krakow, Poland* [H]
14 *Department of Physics, Jagellonian University, Cracow, Poland*
15 *Deutsches Elektronen-Synchrotron DESY, Hamburg, Germany*
16 *Deutsches Elektronen-Synchrotron DESY, Zeuthen, Germany*
17 *INFN Florence, Florence, Italy* [B]
18 *University and INFN Florence, Florence, Italy* [B]
19 *Fakultät für Physik der Universität Freiburg i.Br., Freiburg i.Br., Germany*
20 *School of Physics and Astronomy, University of Glasgow, Glasgow, United Kingdom* [D]
21 *Department of Engineering in Management and Finance, Univ. of the Aegean, Chios, Greece*
22 *Hamburg University, Institute of Experimental Physics, Hamburg, Germany* [I]
23 *Imperial College London, High Energy Nuclear Physics Group, London, United Kingdom* [D]
24 *Institute of Particle and Nuclear Studies, KEK, Tsukuba, Japan* [J]
25 *Institute of Physics and Technology of Ministry of Education and Science of Kazakhstan, Almaty, Kazakhstan*
26 *Institute for Nuclear Research, National Academy of Sciences, Kyiv, Ukraine*
27 *Department of Nuclear Physics, National Taras Shevchenko University of Kyiv, Kyiv, Ukraine*
28 *Kyungpook National University, Center for High Energy Physics, Daegu, South Korea* [K]
29 *Institut de Physique Nucléaire, Université Catholique de Louvain, Louvain-la-Neuve, Belgium* [L]
30 *Departamento de Física Teórica, Universidad Autónoma de Madrid, Madrid, Spain* [M]
31 *Department of Physics, McGill University, Montréal, Québec, Canada H3A 2T8* [N]
32 *Meiji Gakuin University, Faculty of General Education, Yokohama, Japan* [J]

33   *Moscow Engineering Physics Institute, Moscow, Russia* [O]

34   *Lomonosov Moscow State University, Skobeltsyn Institute of Nuclear Physics, Moscow, Russia* [P]

35   *Max-Planck-Institut für Physik, München, Germany*

36   *NIKHEF and University of Amsterdam, Amsterdam, Netherlands* [Q]

37   *Physics Department, Ohio State University, Columbus, Ohio 43210, USA* [A]

38   *Department of Physics, University of Oxford, Oxford, United Kingdom* [D]

39   *INFN Padova, Padova, Italy* [B]

40   *Dipartimento di Fisica dell' Università and INFN, Padova, Italy* [B]

41   *Department of Physics, Pennsylvania State University, University Park, Pennsylvania 16802, USA* [F]

42   *Polytechnic University, Tokyo, Japan* [J]

43   *Dipartimento di Fisica, Università 'La Sapienza' and INFN, Rome, Italy* [B]

44   *Rutherford Appleton Laboratory, Chilton, Didcot, Oxon, United Kingdom* [D]

45   *Raymond and Beverly Sackler Faculty of Exact Sciences, School of Physics, Tel Aviv University, Tel Aviv, Israel* [R]

46   *Department of Physics, Tokyo Institute of Technology, Tokyo, Japan* [J]

47   *Department of Physics, University of Tokyo, Tokyo, Japan* [J]

48   *Tokyo Metropolitan University, Department of Physics, Tokyo, Japan* [J]

49   *Università di Torino and INFN, Torino, Italy* [B]

50   *Università del Piemonte Orientale, Novara, and INFN, Torino, Italy* [B]

51   *Department of Physics, University of Toronto, Toronto, Ontario, Canada M5S 1A7* [N]

52   *Physics and Astronomy Department, University College London, London, United Kingdom* [D]

53   *Faculty of Physics, University of Warsaw, Warsaw, Poland*

54   *National Centre for Nuclear Research, Warsaw, Poland*

55   *Department of Particle Physics and Astrophysics, Weizmann Institute, Rehovot, Israel*

56   *Department of Physics, University of Wisconsin, Madison, Wisconsin 53706, USA* [A]

57   *Department of Physics, York University, Ontario, Canada M3J 1P3* [N]

^{a} now at University of Salerno, Italy

^{b} now at Queen Mary University of London, United Kingdom

^{c} also funded by Max Planck Institute for Physics, Munich, Germany

^{d} also Senior Alexander von Humboldt Research Fellow at Hamburg University, Institute of Experimental Physics, Hamburg, Germany

^{e} also at Cracow University of Technology, Faculty of Physics, Mathematics and Applied Computer Science, Poland

^{f} supported by the research grant No. 1 P03B 04529 (2005-2008)

^{g} partially supported by the Polish National Science Centre projects DEC-2011/01/B/ST2/03643 and DEC-2011/03/B/ST2/00220

^{h} now at Rockefeller University, New York, NY 10065, USA

^{i} now at DESY group FS-CFEL-1

^{j} now at Institute of High Energy Physics, Beijing, China

^{k} now at DESY group FEB, Hamburg, Germany

^{l} also at Moscow State University, Russia

^{m} now at University of Liverpool, United Kingdom

^{n} now at CERN, Geneva, Switzerland

^{o} also affiliated with University College London, UK

^{p} now at Goldman Sachs, London, UK

^{q} also at Institute of Theoretical and Experimental Physics, Moscow, Russia

^{r} also at FPACS, AGH-UST, Cracow, Poland

^{s} partially supported by Warsaw University, Poland

^{t} supported by the Alexander von Humboldt Foundation

^{u} now at Istituto Nazionale di Fisica Nucleare (INFN), Pisa, Italy

^{v} now at Haase Energie Technik AG, Neumünster, Germany

^{w} now at Department of Physics, University of Bonn, Germany

^{x} also affiliated with DESY, Germany

^{y} also at University of Tokyo, Japan

^{z} now at Kobe University, Japan

† deceased

^{aa} supported by DESY, Germany

^{ab} member of National Technical University of Ukraine, Kyiv Polytechnic Institute, Kyiv, Ukraine

^{ac} member of National Technical University of Ukraine, Kyiv, Ukraine

^{ad} now at DESY ATLAS group

^{ae} member of National University of Kyiv - Mohyla Academy, Kyiv, Ukraine

^{af} Alexander von Humboldt Professor; also at DESY and University of Oxford

^{ag} STFC Advanced Fellow

^{ah} now at LNF, Frascati, Italy

^{ai} This material was based on work supported by the National Science Foundation, while working at the Foundation.

^{aj} also at Max Planck Institute for Physics, Munich, Germany, External Scientific Member

[ak] now at Tokyo Metropolitan University, Japan

[al] now at Nihon Institute of Medical Science, Japan

[am] now at Osaka University, Osaka, Japan

[an] also at Łódź University, Poland

[ao] member of Łódź University, Poland

[ap] now at Department of Physics, Stockholm University, Stockholm, Sweden

1   Introduction

The measurement of charm production in deep inelastic ep scattering (DIS) is a powerful tool to study quantum chromodynamics (QCD) and the proton structure. In leading-order QCD, charm production occurs through the boson–gluon fusion (BGF) process $\gamma^* g \to c\bar{c}$, which is directly sensitive to the gluon content of the proton. Different approaches to the calculation of the heavy-quark contribution to the proton structure functions are currently used in global analyses of parton density functions (PDFs) [1–4]. Comparisons to measurements of charm production in DIS provide direct tests of these approaches [5]. It has also been shown recently that a combined analysis of charm production and inclusive DIS data can provide a competitive determination of the charm-quark mass [5–7].

Several measurements of charm production in DIS have been performed at HERA, exploiting reconstructed D^0 [8], $D^\pm$ [8–10] and $D^{*\pm}$ [11–17] mesons, semi-leptonic decays [18], and inclusive lifetime methods [19, 20] to tag charm. In this paper, a new high-statistics measurement of $D^{*\pm}$ production via the reaction

$$ e(k)\, p(P) \; \to \; e'(k')\, D^{*\pm}(p^{D^*})\, X $$

is presented. The symbols in parenthesis represent the four-momenta of the incoming (k) and outgoing electron (k'), of the incoming proton (P), and of the produced $D^{*\pm}$ (p^{D^*}). The measurement is performed for photon virtualities, $Q^2 \equiv -q^2 = -(k' - k)^2$, in the range $5 < Q^2 < 1000$ GeV^2 and for inelasticities, $y \equiv (P \cdot q)/(P \cdot k)$, in the range $0.02 < y < 0.7$.

The D^{*+} mesons[1] were reconstructed through the decay $D^{*+} \to D^0 \pi^+$ with $D^0 \to K^- \pi^+$. Differential cross sections are presented as a function of Q^2, y, the Bjorken-x variable, and of the fraction of the exchanged-photon energy transferred to the D^{*+} meson in the proton rest frame, $z^{D^*} \equiv (P \cdot p^{D^*})/(P \cdot q)$, as well as of the D^{*+} pseudorapidity, η^{D^*}, and the transverse momentum, $p_T^{D^*}$, in the laboratory frame [2].

Double-differential cross sections in Q^2 and y are presented and used to extract the charm contribution to the proton structure functions in the form of the reduced charm cross section, $\sigma_{\text{red}}^{c\bar{c}}$. Previous measurements and theoretical calculations are compared to the results.

---

[1] Hereafter the charge conjugated states are implied.

[2] The ZEUS coordinate system is a right-handed Cartesian system, with the Z axis pointing in the proton beam direction, referred to as the "forward direction", and the X axis pointing towards the centre of HERA. The coordinate origin is at the nominal interaction point. The pseudorapidity is defined as $\eta = -\ln\left(\tan\frac{\theta}{2}\right)$, where the polar angle, θ, is measured with respect to the proton beam direction.

2 Experimental set-up

The measurement was based on $e^\pm p$ collisions collected with the ZEUS detector at HERA in the period 2004–2007 with an electron[3] beam energy, E_e, of 27.5 GeV and a proton beam energy, E_p, of 920 GeV, corresponding to a centre-of-mass energy $\sqrt{s} = 318$ GeV. The corresponding integrated luminosity, $\mathcal{L} = 363 \pm 7$ pb^{-1}, is four times larger than that used for the previous ZEUS measurement [11].

A detailed description of the ZEUS detector can be found elsewhere [21]. In the kinematic range of the analysis, charged particles were tracked in the central tracking detector (CTD) [22] and in the microvertex detector (MVD) [23]. These components operated in a magnetic field of 1.43 T provided by a thin superconducting solenoid. The CTD consisted of 72 cylindrical drift chamber layers, organised in nine superlayers covering the polar-angle region $15° < \theta < 164°$. The MVD consisted of a barrel (BMVD) and a forward (FMVD) section with three cylindrical layers and four vertical planes of single-sided silicon strip sensors in the BMVD and FMVD respectively. The BMVD provided polar-angle coverage for tracks crossing the three layers from 30° to 150°. The FMVD extended the polar-angle coverage in the forward region down to 7°. For CTD–MVD tracks that pass through all nine CTD superlayers, the momentum resolution was $\sigma(p_T)/p_T = 0.0029p_T \oplus 0.0081 \oplus 0.0012/p_T$, with p_T in GeV.

The high-resolution uranium–scintillator calorimeter (CAL) [24] consisted of three parts: the forward, the barrel, and the rear (RCAL) calorimeters. Under test-beam conditions, the CAL single-particle relative energy resolutions were $\sigma(E)/E = 0.18/\sqrt{E}$ for electrons and $\sigma(E)/E = 0.35/\sqrt{E}$ for hadrons, with E in GeV. The energy of electrons hitting the RCAL was corrected for the presence of dead material using the rear presampler detector [25] and the small angle rear tracking detector (SRTD) [26].

The luminosity was measured using the Bethe–Heitler reaction $ep \to e\gamma p$ by a luminosity detector which consisted of two independent systems: a lead–scintillator calorimeter [27] and a magnetic spectrometer [28].

3 QCD calculations

Cross sections for heavy-quark production in DIS were calculated at next-to-leading order (NLO), i.e. $O(\alpha_s^2)$, in the fixed-flavour-number scheme (FFNS), in which only light flavours and gluons are present as partons in the proton and heavy quarks are produced

---

[3] Hereafter "electron" refers to both electrons and positrons unless otherwise stated.

in the hard interaction [29]. The program HVQDIS [30, 31] was used to compute single- and double-differential D^{*+} cross sections.

The parameters used as input to HVQDIS are listed below, together with the variations used to evaluate the uncertainty on the theoretical prediction:

- charm-quark pole mass: $m_c = 1.50 \pm 0.15\,\text{GeV}$;

- renormalisation (μ_R) and factorisation (μ_F) scales: $\mu_R = \mu_F = \sqrt{Q^2 + 4m_c^2}$, varied independently up and down by a factor two;

- strong coupling constant in the three-flavour FFNS: $\alpha_s^{\text{nf}=3}(M_Z) = 0.105 \pm 0.002$;

- the PDFs and their uncertainties, taken from a FFNS variant [5] of the HERAPDF1.0 fit [32]. The central PDF set was obtained from a fit performed using the same values of m_c, μ_R, μ_F and α_s as used in the HVQDIS program. For each variation of these parameters in HVQDIS, a different PDF set was used, in which the parameters were varied consistently.

The NLO calculation provided differential cross sections for charm quarks. The fragmentation model described in a previous publication [5] was used to compare to the measured D^{*+} cross sections. This model is based on the fragmentation function of Kartvelishvili et al. [33], controlled by the parameter α_K, to describe the fraction of the charm momentum transferred to the D^{*+} mesons. It also implements a transverse fragmentation component by assigning to the D^{*+} meson a transverse momentum, k_T, with respect to the charm-quark direction. The uncertainty on the fragmentation model was estimated by varying α_K and the average k_T according to the original prescription [5]. The fraction of charm quarks hadronising into D^{*+} mesons was set to $f(c \to D^{*+}) = 0.2287 \pm 0.0056$ [34].

For the inclusive cross section, theoretical predictions were also obtained in the generalised-mass variable-flavour-number scheme (GM-VFNS). In this scheme, charm quarks are treated as massive particles for $Q^2 \le m_c^2$ and as massless partons for $Q^2 \gg m_c^2$, interpolating in the intermediate region [35–37]. The calculation was performed using the Roberts–Thorne (RT) "standard" [38, 39] variant of the GM-VFNS at NLO, corresponding to $O(\alpha_s^2)$ for the $Q^2 \le m_c^2$ part and to $O(\alpha_s)$ for the $Q^2 \gg m_c^2$ part. PDFs obtained from the HERAPDF1.5 [40] fit to inclusive HERA data were used. The central prediction was obtained for $m_c = 1.5$ GeV. To evaluate the theoretical uncertainty, the calculation was repeated varying the PDF set and its parameters according to the systematic variations associated with the HERAPDF1.5 fit. The dominant source of uncertainty was the charm-quark mass, which was varied in the range $1.35 < m_c < 1.65\,\text{GeV}$.

4 Monte Carlo samples

Monte Carlo (MC) samples were used to calculate the experimental acceptance and to estimate the background contamination. MC samples of charm and beauty DIS events were generated using RAPGAP 3.00 [41]. The main sample consisted of events generated according to the LO BGF process. Radiative QED corrections to the BGF process were included through HERACLES 4.6 [42]. Additional RAPGAP samples were generated for diffractive charm production and for the resolved-photon processes $gg \to c\bar{c}$ and $cg \to cg$, in which one of the incoming partons originates from the exchanged photon. Charm photoproduction was simulated using PYTHIA 6.2 [43].

Both RAPGAP and PYTHIA use parton showers to simulate higher-order QCD effects and use the PYTHIA/JETSET hadronisation model [43]. All samples were generated using the CTEQ5L [44] proton PDFs and, for resolved-photon processes, the GRV-G LO [45] photon PDFs. The diffractive samples were generated using the "H1 fit 2" [46] diffractive PDFs. The heavy-quark masses were set to $m_c = 1.5\,\mathrm{GeV}$ and $m_b = 4.75\,\mathrm{GeV}$. Masses, widths and lifetimes of charmed mesons were taken from PDG2010 [47].

The MC samples correspond to about four times the luminosity of the data and were passed through a full simulation of the ZEUS detector based on GEANT 3.21 [48]. They were then subjected to the same trigger criteria and reconstructed with the same programs as used for the data.

5 Event selection and signal extraction

5.1 DIS event selection

A three-level trigger system was used to select DIS events online [21, 49, 50] by requiring electromagnetic energy deposits in the CAL at the first level and applying loose DIS selection criteria at the second and third levels.

Offline, the hadronic system was reconstructed using energy-flow objects (EFOs) [51] which combine tracking and calorimeter information. The electron was identified using a neural-network algorithm [52]. The kinematical variables Q^2, y, and x were reconstructed using the Σ method [53]. The variable z^{D^*} was reconstructed according to $z^{D^*} = (E^{D^*} - p_Z^{D^*})/(2E_e y_{\mathrm{JB}})$, where y_{JB} is the inelasticity reconstructed with the Jacquet-Blondel method [54] and E^{D^*} and $p_Z^{D^*}$ are the D^{*+} energy and longitudinal momentum, respectively.

The following criteria were applied to select DIS events [55]:

- $E_{e'} > 10\,\mathrm{GeV}$, where $E_{e'}$ is the energy of the scattered electron;

- $y_e < 0.7$, $y_{\mathrm{JB}} > 0.02$, where y_e is the inelasticity reconstructed from the scattered electron;

- $40 < E - P_Z < 70\,\mathrm{GeV}$, where $E - P_Z$ is the global difference of energy and longitudinal momentum, obtained by summing the electron and the hadronic final state, which is expected to be $2E_e = 55\,\mathrm{GeV}$ for fully contained events;

- the Z position of the primary vertex, Z_{vtx}, was required to be in the range $|Z_{\mathrm{vtx}}| < 30\,\mathrm{cm}$;

- the impact point of the scattered electron on the RCAL was required to lie outside a square region around the beam-pipe hole: $|X_e| > 15$ cm or $|Y_e| > 15$ cm;

- $5 < Q^2 < 1000\ \mathrm{GeV}^2$, where Q^2 is reconstructed with the Σ method.

5.2 Selection of D^{*+} candidates and signal extraction

The D^{*+} mesons were identified using the decay channel $D^{*+} \to D^0 \pi_s^+$ with the subsequent decay $D^0 \to K^- \pi^+$, where π_s^+ refers to a low-momentum ("slow") pion accompanying the D^0.

Tracks from the D^{*+} decay products were required to have at least one hit in the MVD or in the inner superlayer of the CTD and to reach at least the third superlayer. Tracks with opposite charge and with transverse momentum $p_T^{K,\pi} > 0.4\,\mathrm{GeV}$ were combined in pairs to form D^0 candidates. The track parameters were improved by fitting the two tracks to a common vertex. Pairs incompatible with coming from the same decay were removed by requiring a distance of closest approach of the two tracks of less than 1 mm, and the χ^2 of the two-track vertex fit smaller than 20 for one degree of freedom. The tracks were alternately assigned the kaon and pion mass and the invariant mass of the pair, $M(K\pi)$, was calculated. Each additional track, with charge opposite to that of the kaon track and a transverse momentum $p_T^{\pi_s} > 0.12\,\mathrm{GeV}$, was assigned the pion mass and combined with the D^0 candidate to form a D^{*+} candidate. The π_s track was then fitted to the primary vertex of the event, obtained exploiting the other tracks reconstructed in the event and the constraint from the average position of the interaction point [8]. The mass difference $\Delta M \equiv M(K\pi\pi_s) - M(K\pi)$ was used to extract the D^{*+} signal. The D^{*+} candidates were required to have $1.80 < M(K\pi) < 1.92\,\mathrm{GeV}$, $143.2 < \Delta M < 147.7\,\mathrm{MeV}$, $1.5 < p_T^{D^*} < 20\,\mathrm{GeV}$ and $|\eta^{D^*}| < 1.5$.

The distribution of $M(K\pi)$ for D^{*+} candidates, without the requirement on $M(K\pi)$, is shown in Fig. 1. Also shown is the distribution of wrong-sign (WS) candidates, obtained by combining two tracks with the same charge. The WS distribution provides an estimate

of combinatorial backgrounds. A clear peak at the D^0 mass is visible in the correct-sign (CS) distribution. The excess of CS candidates at masses below the D^0 peak is due to partly-reconstructed D^0 decays, mostly $D^0 \rightarrow K^- \pi^+ \pi^0$.

The distribution of ΔM for D^{*+} candidates, without the requirement on ΔM, is shown in Fig. 2. A clear D^{*+} peak is seen. The D^{*+} signal was extracted by subtracting the background estimate from the number of candidates in the signal window $143.2 < \Delta M < 147.7\,\text{MeV}$. The background estimate was obtained by fitting simultaneously the CS and WS distributions to the parametrisation

$$\text{WS}: \quad f_\text{ws}(\zeta) = A\,\zeta^B\,e^{-C\zeta},$$
$$\text{CS}: \quad f_\text{cs}(\zeta) = D\,f_\text{ws}(\zeta),$$

where A, B, C, D are free parameters of the fit [56] and $\zeta = \Delta M - m_{\pi^+}$. The fit was performed in the region $\Delta M < 168\,\text{MeV}$. The region with a possible signal contribution, $140 < \Delta M < 150\,\text{MeV}$, was removed from the fit to the CS distribution. The parameter D, which represents the normalisation of the CS background with respect to the WS distribution, is slightly larger than unity, $D = 1.021 \pm 0.005$. This is consistent with the MC estimation of the additional combinatorial background component in the CS distribution due to real $D^0 \rightarrow K\pi$ decays associated with a random track to form a CS D^{*+} candidate. The total signal is $N_\text{data}^{D^{*\pm}} = 12893 \pm 185$.

The amount of signal lost due to the tails of the D^0 mass peak leaking outside the $M(K\pi)$ window was estimated by enlarging the mass window to $1.7 < M(K\pi) < 2.0\,\text{GeV}$. The fraction of additional D^{*+} found within the enlarged window was 13%, including the contribution from partly reconstructed D^0. This fraction, as well as its dependence on $p_T^{D^*}$ and η^{D^*} and on the width of the $M(K\pi)$ window, was found to be well reproduced by MC. The signal in the tails of the D^{*+} peak outside the ΔM window was estimated similarly, enlarging the signal window to $140 < \Delta M < 150\,\text{MeV}$. The fraction of additional D^{*+} was 6% on average, with a dependence on the transverse momentum of the slow pion, due to the momentum and angular resolution degrading at low $p_T^{\pi s}$. This effect is not completely reproduced by the MC. An acceptance correction [55] dependent on $p_T^{\pi s}$ was then applied, ranging from $\approx 10\%$ at $p_T^{\pi s} = 0.12\,\text{GeV}$ to $\approx 1\%$ at large $p_T^{\pi s}$.

6   Cross-section extraction

The differential cross sections, $d\sigma_\text{vis}/d\xi$, for producing a D^{*+} in the "visible" phase space $1.5 < p_T^{D^*} < 20\,\text{GeV}$, $|\eta^{D^*}| < 1.5$, $5 < Q^2 < 1000\,\text{GeV}^2$ and $0.02 < y < 0.7$ was obtained as

$$\frac{d\sigma_\text{vis}}{d\xi} = \frac{N_\text{data}^{D^*} - N_{\gamma p}^{D^*}}{\Delta\xi \cdot \mathcal{A} \cdot BR \cdot \mathcal{L}} \cdot C_r,$$

where $N_{\text{data}}^{D^*}$ is the signal extracted in a bin of a given variable ξ, $N_{\gamma p}^{D^*}$ is the photoproduction background, $\Delta\xi$ is the bin size, $\mathcal{A}$ is the acceptance, $BR = \mathcal{B}(D^{*+} \to D^0\pi^+) \times \mathcal{B}(D^0 \to K^-\pi^+) = 0.0263 \pm 0.0004$ [57] is the branching ratio, $\mathcal{L}$ is the integrated luminosity and C_r is the QED radiative correction.

The background from charm photoproduction ($Q^2 < 1.5$ GeV^2) was evaluated using the photoproduction MC sample, normalised to the luminosity using the cross sections previously measured by ZEUS [58].

The acceptance, $\mathcal{A}$, was calculated as the ratio between the number of reconstructed and generated D^{*+} in the bin, using a signal MC based on a mix of charm and beauty production. The beauty MC was normalised to 1.6 times the cross section given by RAPGAP, consistent with ZEUS measurements [18, 59–61]. The charm MC contained non-diffractive and diffractive components, summed according to the relative cross sections as given by RAPGAP. The normalisation of the charm MC was adjusted such that the sum of all the MC components reproduced the number of D^{*+} mesons in the data. Resolved-photon processes were not included. They were only used for systematic checks. The η^{D^*} and $p_T^{D^*}$ distributions of the charm MC were reweighted [55] to improve the agreement with data, with the $p_T^{D^*}$ weights dependent on Q^2.

The acceptance as determined by the MC was corrected to account for imperfections in the simulation of the trigger and track-reconstruction efficiencies. One of the main sources of track-reconstruction inefficiency for charged pions and kaons were hadronic interactions in the material between the interaction point and the CTD. This effect was studied using special tracks from $ep \to e\rho^0$ with $\rho^0 \to \pi^+\pi^-$ events, reconstructed from MVD hit information alone [62]. For these tracks, an extension into the CTD was searched for. In addition, the p_T dependence of the tracking efficiency was studied by exploiting the isotropic angular distribution of pions from K_S^0 decays. The studies showed that the MC slightly underestimated the effect of nuclear interactions. For central pions with $p_T \approx 1$ GeV, the track-reconstruction inefficiency due to hadronic interactions was measured to be $(7 \pm 1)\%$ while the MC predicted 5%. The track-efficiency correction was applied as a function of η and p_T of each track. For $p_T > 1.5$ GeV, no correction was necessary.

The acceptance ranges from $\mathcal{A} \approx 10\%$ in the lowest $p_T^{D^*}$ and Q^2 bins to $\mathcal{A} \approx 45\%$ in the highest $p_T^{D^*}$ and Q^2 bins. Fig. 3 shows $N_{\text{data}}^{D^*}/\Delta\xi$ for $\xi = p_T^{D^*}, \eta^{D^*}, Q^2, y$ and z^{D^*}. The sum of the different MC samples is compared to the data. The agreement is satisfactory.

The cross sections were corrected to the QED Born level, using a running coupling constant $\alpha_{\text{em}}(Q^2)$, such that they can be compared directly to the QCD predictions from the HVQDIS program. The radiative corrections were obtained as $C_r = \sigma_{\text{vis}}^{\text{Born}}/\sigma_{\text{vis}}^{\text{rad}}$, where $\sigma_{\text{vis}}^{\text{Born}}$ is the RAPGAP cross section with the QED corrections turned off but keeping α_{em} running and $\sigma_{\text{vis}}^{\text{rad}}$ is the RAPGAP cross section with the full QED corrections, as in the

standard MC samples.

7 Systematic uncertainties

The experimental systematic uncertainties are listed below [55], with their typical effect on the measured cross sections is given in parenthesis:

δ_1 energy-scale uncertainty on the hadronic system of $\pm2\%$ ($\pm1\%$, up to $\pm10\%$ at low y);

δ_2 electron energy-scale uncertainty of $\pm1\%$ [63] ($\pm1\%$, up to $\pm7\%$ at low y);

δ_3 alignment uncertainty on the electron impact point on the RCAL, estimated by varying the cut on the electron position in the MC by ±2 mm separately for the X_e and Y_e coordinates [63] ($\pm7\%$ at low Q^2 and low y, negligible at large Q^2);

δ_4 uncertainty on the position of the electron impact point on the RCAL due to imperfections in the simulation of the shower shape and of the detector resolution, estimated by loosening the cut on the electron position by 1 cm ($|X_e| > 14$ cm or $|Y_e| > 14$ cm) both in data and in MC (up to $\pm10\%$ at low y and low Q^2, negligible at large Q^2);

δ_5 uncertainty on the background shape in ΔM, estimated by replacing the function $f_{\rm cs}(\zeta)$ by $f'_{\rm cs}(\zeta) = A\zeta^{\frac{2}{3}} + B\zeta + C\zeta^{\frac{1}{2}}$ ($+0.3\%$);

δ_6 a further uncertainty on the background shape, evaluated by reducing the fit range from $\Delta M < 168\,\mathrm{MeV}$ to $\Delta M < 165\,\mathrm{MeV}$ ($+0.5\%$);

δ_7 uncertainty on the amount of signal outside the ΔM window, evaluated by varying the $p_T^{\pi s}$-dependent correction by its uncertainty ($\pm1.5\%$, up to $\pm3\%$ at low p_T);

δ_8 uncertainty on the amount of signal outside the $M(K\pi)$ window, estimated by comparing data and MC in an enlarged mass range ($+2\%$);

δ_9 uncertainty on the track-efficiency, evaluated by varying the track efficiency correction applied to MC by the associated uncertainty ($\pm2\%$);

δ_{10} uncertainty on the trigger efficiency, evaluated using independent triggers ($\pm0.5\%$);

δ_{11} statistical uncertainty on the calculation of the acceptance ($\pm1\%$);

δ_{12} uncertainty on the normalisation of the beauty MC of $\pm50\%$ to cover the range allowed by ZEUS measurements [59, 61] ($\pm0.3\%$);

δ_{13} uncertainty on the normalisation of the photoproduction MC of $\pm100\%$ (up to $\pm3\%$ at high y, but negligible elsewhere);

δ_{14} uncertainty on the normalisation of the diffractive charm MC of $\pm 50\%$ to cover the range allowed by data–MC comparison and by previous ZEUS results [64] (up to $\pm 4.5\%$ at low y, but negligible elsewhere);

δ_{15} uncertainty due to the resolved-photon component, evaluated by adding the resolved-photon samples to the charm MC normalised according to the generator cross section $(+2\%)$;

δ_{16} uncertainty on the MC reweighting as a function of $p_T^{D^*}$ and Q^2, which was varied by $\pm 50\%$ ($\pm 2\%$);

δ_{17} uncertainty on the MC reweighting as a function of η^{D^*} which was replaced by a MC reweighting as a function of y (from -2% to $+3\%$, depending on y);

δ_{18} uncertainty on the integrated luminosity of $\pm 1.9\%$;

δ_{19} uncertainty on the branching ratio BR of $\pm 1.5\%$.

All the systematic uncertainties, except the overall normalisations δ_{18} and δ_{19}, were added in quadrature to the statistical uncertainties to obtain the total error bars in the figures.

8 Results

Single- and double-differential cross sections have been measured in the phase space

$$5 < Q^2 < 1000 \,\text{GeV}^2; \ 0.02 < y < 0.7; \ 1.5 < p_T^{D^*} < 20 \,\text{GeV}; \ |\eta^{D^*}| < 1.5.$$

Differential cross sections in $p_T^{D^*}$, η^{D^*} and z^{D^*} are reported in Tables 1–3 and in Fig. 4. The cross section decreases steeply with $p_T^{D^*}$ and is almost constant in η^{D^*}. The NLO calculations based on HVQDIS and the RAPGAP MC implementing the leading-order BGF process are compared to the data. As the RAPGAP MC is based on leading-order matrix elements, it is not expected to estimate the normalisation correctly. Therefore the RAPGAP prediction was normalised to the data, scaling it by 1.1, to allow a direct comparison of the shapes. The data are well described by the NLO calculation and by RAPGAP with the exception of the shape in z^{D^*}, which is not well reproduced by the NLO calculation, suggesting possible imperfections in the fragmentation model.

Differential cross sections in Q^2, y and x are reported in Tables 4–6 and in Fig. 5. The results are reasonably well described by the NLO calculation. The MC predictions reproduce the shapes of the data, except for the high-Q^2 tail, where the MC prediction is too high, and for $d\sigma/dy$, where the prediction is too low at low y and too high at large y. These imperfections in the MC are to be expected in the absence of higher-order terms in RAPGAP.

Visible cross sections in two-dimensional bins of Q^2 and y, σ_{vis}, are given in Table 7. The corresponding bin-averaged double-differential cross sections are shown in Figs. 6 and 7. The values of the individual systematic uncertainties on the double-differential cross sections are given in Table 8. Measurements performed in the same phase space by the H1 Collaboration [16, 17], which are the most precise previous measurement of D^{*+} production in DIS, are compared to the present results. The two data sets are in agreement and have similar precision. The double-differential cross sections are well described by the NLO calculation.

In a previous ZEUS measurement [11], a possible excess in the D^{*+} yield in e^-p collisions was observed with respect to e^+p collisions. The ratio of observed rates, increasing with Q^2, was $r^{e^-p}/r^{e^+p} = 1.67 \pm 0.21(\text{stat.})$ for $40 < Q^2 < 1000\,\mathrm{GeV}^2$. The measurement was based on a luminosity of 17 (65) pb^{-1} of e^-p (e^+p) collisions. The present measurement is based on an independent data set, consisting of 187 (174) pb^{-1} of e^-p (e^+p) collisions. Fig. 8 shows the cross-section ratio as a function of Q^2. Only statistical uncertainties are shown since systematic effects mostly cancel in the ratio. No deviation from unity is observed, confirming the original interpretation of the e^-p excess as a statistical fluctuation.

9   Charm reduced cross sections

The reduced cross section for charm, $\sigma_{\mathrm{red}}^{c\bar{c}}$, and the charm contribution to the proton structure functions, $F_2^{c\bar{c}}$ and $F_L^{c\bar{c}}$, are defined as:

$$\frac{d^2\sigma^{c\bar{c}}}{dx\,dQ^2} = \frac{2\pi\alpha_{em}^2}{xQ^4}\,Y_+\,\sigma_{\mathrm{red}}^{c\bar{c}}(x, Q^2, s),$$

$$\sigma_{\mathrm{red}}^{c\bar{c}}(x, Q^2, s) = F_2^{c\bar{c}}(x, Q^2) - \frac{y^2}{Y_+}F_L^{c\bar{c}}(x, Q^2),$$

where $Y_+ = 1 + (1 - y)^2$.

The HVQDIS program was used to extrapolate the measured visible D^{*+} cross sections in bins of y and Q^2, σ_{vis}, to the full phase space:

$$\sigma_{\mathrm{red}}^{c\bar{c}}(x, Q^2) = \left(\sigma_{\mathrm{vis}} - \sigma_{\mathrm{vis}}^{\mathrm{beauty}}\right)\left(\frac{\sigma_{\mathrm{red, HVQDIS}}^{c\bar{c}}(x, Q^2)}{\sigma_{\mathrm{vis, HVQDIS}}}\right),$$

where $\sigma_{\mathrm{vis}}^{\mathrm{beauty}}$ is the beauty contribution as predicted by the RAPGAP MC, normalised as discussed in Section 6, and $\sigma_{\mathrm{red, HVQDIS}}^{c\bar{c}}$, $\sigma_{\mathrm{vis, HVQDIS}}$ are the charm reduced and the visible D^{*+} cross sections, respectively, as given by HVQDIS. The reference values of x and Q^2 were chosen close to the average x and Q^2 of the bins. The kinematic acceptance of the

visible phase space, defined as $\mathcal{A}_{ps} = \sigma_{\text{vis}}/(\sigma^{c\bar{c}} \cdot 2\,f(c \to D^{*+}))$, where $\sigma^{c\bar{c}}$ is the charm production total cross section in the y and Q^2 bin, ranges from 17% to 64%, depending on the bin.

Following the method used in the previously published combination of ZEUS and H1 results [5], the HVQDIS and fragmentation variations described in Section 3 were used to determine the theoretical uncertainty on the extraction of $\sigma_{\text{red}}^{c\bar{c}}$. The scales μ_R and μ_F were varied simultaneously rather than independently as in the theoretical uncertainty for the differential cross sections. An additional uncertainty originates from the subtracted beauty component that was varied by $\pm 50\%$. The theoretical uncertainties due the extrapolation on $\sigma_{\text{red}}^{c\bar{c}}(x, Q^2)$ are given in Table 9. The experimental part of the uncertainties on $\sigma_{\text{red}}^{c\bar{c}}(x, Q^2)$ is defined as the quadratic sum of the statistical and the experimental systematic uncertainties described in Section 7.

The results are reported in Table 10 and are shown in Fig. 9. The combined result based on previous H1 and ZEUS charm measurements [5] and a recent ZEUS measurement with D^+ mesons [9], not included in the combined results, are also shown. All three measurements are in good agreement. The D^* measurement has a precision close to that of the combined result in some parts of the phase space. The GM-VFNS calculation, based on the HERAPDF1.5 parton-density fit to inclusive HERA data, is compared to the present measurement and shown in Fig. 10. The uncertainty on the prediction is dominated by the charm-quark mass. The prediction is in good agreement with the data.

10   Conclusions

Differential cross sections for the production of $D^{*\pm}$ mesons in DIS have been measured with the ZEUS detector in the kinematic range

$$5 < Q^2 < 1000\,\text{GeV}^2;\; 0.02 < y < 0.7;\; 1.5 < p_T^{D^*} < 20\,\text{GeV};\; |\eta^{D^*}| < 1.5,$$

using data from an integrated luminosity of $363\,\text{pb}^{-1}$. The new data represents one of the most precise measurements of charm production in DIS obtained to date. The data are reasonably well described by NLO QCD calculations and are in agreement with previously published results.

The measurements have been used to extract the reduced cross sections for charm $\sigma_{\text{red}}^{c\bar{c}}$. A GM-VFNS calculation based on a PDF fit to inclusive DIS HERA data agrees well with the results. This demonstrates a consistent description of charm and inclusive data within the NLO QCD framework.

Acknowledgements

References

[1] S. Kretzer et al., Phys. Rev. **D 69**, 114005 (2004).

[2] A.D. Martin et al., Eur. Phys. J. **C 63**, 189 (2009).

[3] S. Alekhin et al., Phys. Rev. **D 81**, 014032 (2010).

[4] R.D. Ball et al., Nucl. Phys. **B 849**, 296 (2011).

[5] H1 and ZEUS Coll., H. Abramowicz et al., Eur. Phys. J. **C 73**, 2311 (2013).

[6] S. Alekhin and S. Moch, Phys. Lett. **B 699**, 345 (2011).

[7] S. Alekhin et al., Phys. Lett. **B 718**, 550 (2012).

[8] ZEUS Coll., S. Chekanov et al., Eur. Phys. J. **C 63**, 171 (2009).

[9] ZEUS Coll., H. Abramowicz et al. (2013). Submitted to JHEP, Preprint DESY-13-028.

[10] ZEUS Coll., H. Abramowicz et al., JHEP **1011**, 009 (2010).

[11] ZEUS Coll., S. Chekanov et al., Phys. Rev. **D 69**, 012004 (2004).

[12] ZEUS Coll., J. Breitweg et al., Phys. Lett. **B 407**, 402 (1997).

[13] ZEUS Coll., J. Breitweg et al., Eur. Phys. J. **C 12**, 35 (2000).

[14] H1 Coll., C. Adloff et al., Phys. Lett. **B 528**, 199 (2002).

[15] H1 Coll., A. Aktas et al., Eur. Phys. J. **C 38**, 447 (2005).

[16] H1 Coll., F.D. Aaron et al., Phys. Lett. **B 686**, 91 (2010).

[17] H1 Coll., F.D. Aaron et al., Eur. Phys. J. **C 71**, 1769 (2011).

[18] ZEUS Coll., S. Chekanov et al., Eur. Phys. J **C 65**, 65 (2010).

[19] H1 Coll., A. Aktas et al., Eur. Phys. J. **C 45**, 23 (2006).

[20] H1 Coll., F.D. Aaron et al., Eur. Phys. J. **C 65**, 89 (2010).

[21] ZEUS Coll., U. Holm (ed.), *The ZEUS Detector*. Status Report (unpublished), DESY (1993), available on `http://www-zeus.desy.de/bluebook/bluebook.html`.

[22] N. Harnew et al., Nucl. Inst. Meth. **A 279**, 290 (1989);
B. Foster et al., Nucl. Phys. Proc. Suppl. **B 32**, 181 (1993);
B. Foster et al., Nucl. Inst. Meth. **A 338**, 254 (1994).

[23] A. Polini et al., Nucl. Inst. Meth. **A 581**, 656 (2007).

[24] M. Derrick et al., Nucl. Inst. Meth. **A 309**, 77 (1991);
A. Andresen et al., Nucl. Inst. Meth. **A 309**, 101 (1991);
A. Caldwell et al., Nucl. Inst. Meth. **A 321**, 356 (1992);
A. Bernstein et al., Nucl. Inst. Meth. **A 336**, 23 (1993).

[25] A. Bamberger et al., Nucl. Inst. Meth. **A 382**, 419 (1996).

[26] A. Bamberger et al., Nucl. Inst. Meth. **A 401**, 63 (1997).

[27] J. Andruszków et al., Preprint DESY-92-066, DESY, 1992;
ZEUS Coll., M. Derrick et al., Z. Phys. **C 63**, 391 (1994);
J. Andruszków et al., Acta Phys. Pol. **B 32**, 2025 (2001).

[28] M. Helbich et al., Nucl. Inst. Meth. **A 565**, 572 (2006).

[29] J. Smith and W.L. van Neerven, Nucl. Phys. **B 374**, 36 (1992).

[30] B.W. Harris and J. Smith, Nucl. Phys. **B 452**, 109 (1995).

[31] B.W. Harris and J. Smith, Phys. Lett. **B 353**, 535 (1995). Erratum-ibid **B 359** (1995) 423.

[32] H1 and ZEUS Coll., F.D. Aaron et al., JHEP **2010**, 1 (2010).

[33] V.G. Kartvelishvili, A.K. Likhoded and V.A. Petrov, Phys. Lett. **B 78**, 615 (1978).

[34] E. Lohrmann, *A summary of charm hadron production fractions* (unpublished) (2011). Available at arXiv:hep-ex/1112.3757.

[35] M.A.G. Aivazis et al., Phys. Rev. **D 50**, 3102 (1994).

[36] M. Buza et al., Nucl. Phys. **B 472**, 611 (1996).

[37] J.C. Collins, Phys. Rev. **D 58**, 094002 (1998).

[38] R.G. Roberts and R.S. Thorne, Phys. Lett. **B 421**, 303 (1998).

[39] R.G. Roberts and R.S. Thorne, Phys. Rev. **D 57**, 6871 (1998).

[40] H1 and ZEUS Coll., HERAPDF1.5. LHPDF grid, available on
`http://www.desy.de/h1zeus/combined_results/index.php?do=proton_structure`;
V. Radescu, *Proceedings of the 35th International Conference of High Energy Physics,* Proceedings of Science, PoS **ICHEP2010**, p. 168. (2010).

[41] H. Jung, Comp. Phys. Comm. **86**, 147 (1995).

[42] A. Kwiatkowski, H. Spiesberger and H.-J. Möhring, Comp. Phys. Comm. **69**, 155 (1992). Also in *Proc. Workshop Physics at HERA*, (eds). W. Buchmüller and G.Ingelman, (DESY, Hamburg, 1991).

[43] T. Sjöstrand, L. Lönnblad and S. Mrenna, Preprint hep-ph/0108264, 2001.

[44] CTEQ Coll., H.L. Lai et al., Eur. Phys. J. **C 12**, 375 (2000).

[45] M. Glück, E. Reya and A. Vogt, Phys. Rev. **D 45**, 3986 (1992).

[46] H1 Coll., C. Adloff et al., Phys. Lett. **B 520**, 191 (2001).

[47] Particle Data Group, K. Nakamura et al., J. Phys. **G 37**, 075021 (2010).

[48] R. Brun et al., GEANT3, Technical Report CERN-DD/EE/84-1, CERN, 1987.

[49] W.H. Smith, K. Tokushuku and L.W. Wiggers, *Proc. Computing in High-Energy Physics (CHEP), Annecy, France, Sept. 1992*, C. Verkerk and W. Wojcik (eds.), p. 222. CERN, Geneva, Switzerland (1992). Also in preprint DESY 92-150B.

[50] P.D. Allfrey et al., Nucl. Inst. Meth. **A 580**, 1257 (2007).

[51] G.M. Briskin, Ph.D. Thesis, Tel Aviv University, Report DESY-THESIS 1998-036 (1998).

[52] H. Abramowicz, A. Caldwell and R. Sinkus, Nucl. Inst. Meth. **A 365**, 508 (1995).

[53] U. Bassler and G. Bernardi, Nucl. Inst. Meth. **A 361**, 197 (1995).

[54] F. Jacquet and A. Blondel, *Proceedings of the Study for an ep Facility for Europe*, U. Amaldi (ed.), p. 391. Hamburg, Germany (1979). Also in preprint DESY-79-48.

[55] O. Bachynska, Ph.D. Thesis, Hamburg University, Report DESY-THESIS 2012-045 (2012).

[56] P. Granet et al., Nucl. Phys. **B 140**, 389 (1978).

[57] Particle Data Group, J. Beringer et al., Phys. Rev. **D 86**, 010001 (2012).

[58] ZEUS Coll., J. Breitweg et al., Phys. Lett. **B 401**, 192 (1997); ZEUS Coll., J. Breitweg et al., Eur. Phys. J. **C 6**, 67 (1999).

[59] ZEUS Coll., S. Chekanov et al., Phys. Lett. **B 599**, 173 (2004).

[60] ZEUS Coll., H. Abramowicz et al., Eur. Phys. J. **C 69**, 347 (2010).

[61] ZEUS Coll., H. Abramowicz et al., Eur. Phys. J. **C 71**, 1573 (2011).

[62] V. Libov, Ph.D. Thesis, Hamburg University (2013).

[63] S. Shimizu, Ph.D. Thesis, KEK, Tokyo University, Report KEK-2009-1, available on http://www-zeus.desy.de/physics/sfe/theses/shimaFL.pdf. (2009).

[64] ZEUS Coll., S. Chekanov et al., Nucl. Phys. **B 672**, 3 (2003).

$p_T^{D^*}$ (GeV)	$\frac{d\sigma}{dp_T^{D^*}}$ (nb/ GeV)	δ_{stat} (%)	δ_{syst} (%)	C_r
1.50 : 1.88	2.16	9.9	$^{+7.0}_{-5.5}$	1.03
1.88 : 2.28	2.30	5.8	$^{+5.4}_{-5.8}$	1.04
2.28 : 2.68	1.95	4.4	$^{+5.0}_{-4.4}$	1.03
2.68 : 3.08	1.63	4.0	$^{+4.7}_{-4.0}$	1.03
3.08 : 3.50	1.22	3.8	$^{+4.9}_{-4.2}$	1.04
3.50 : 4.00	9.71×10^{-1}	3.4	$^{+4.4}_{-3.7}$	1.03
4.00 : 4.75	6.26×10^{-1}	3.2	$^{+4.2}_{-3.5}$	1.05
4.75 : 6.00	3.32×10^{-1}	3.0	$^{+4.3}_{-3.7}$	1.01
6.00 : 8.00	1.21×10^{-1}	4.1	$^{+4.1}_{-3.8}$	1.06
8.00 : 11.00	3.31×10^{-2}	6.0	$^{+4.4}_{-3.7}$	1.11
11.00 : 20.00	3.60×10^{-3}	12	$^{+5.3}_{-6.1}$	1.11

Table 1: *Differential cross section for $D^{*\pm}$ production in $p_T^{D^*}$, in the kinematic range $5 < Q^2 < 1000 \ GeV^2$, $0.02 < y < 0.7$, $1.5 < p_T^{D^*} < 20 \ GeV$, $|\eta^{D^*}| < 1.5$. The columns list the bin range, the bin-averaged differential cross section, the statistical, δ_{stat}, and systematic, δ_{syst}, uncertainties, and the QED correction factors, C_r. The overall normalization uncertainties from the luminosity ($\pm 1.9\%$) and branching ratio of the $D^{*\pm}$ decay channel ($\pm 1.5\%$) are not included.*

η^{D^*}	$\frac{d\sigma}{d\eta^{D^*}}$ (nb)	δ_{stat} (%)	δ_{syst} (%)	C_r
$-1.50 : -1.25$	1.48	7.5	$^{+6.8}_{-6.7}$	1.06
$-1.25 : -1.00$	1.66	5.4	$^{+5.6}_{-5.3}$	1.05
$-1.00 : -0.75$	1.61	4.9	$^{+6.1}_{-4.4}$	1.05
$-0.75 : -0.50$	1.85	4.2	$^{+4.6}_{-3.8}$	1.03
$-0.50 : -0.25$	1.94	4.2	$^{+4.3}_{-3.5}$	1.03
$-0.25 : 0.00$	2.02	4.0	$^{+4.3}_{-3.7}$	1.04
$0.00 : 0.25$	1.90	4.4	$^{+4.2}_{-3.4}$	1.04
$0.25 : 0.50$	1.97	4.4	$^{+4.3}_{-3.3}$	1.05
$0.50 : 0.75$	1.96	4.7	$^{+4.5}_{-3.6}$	1.03
$0.75 : 1.00$	2.02	4.9	$^{+4.8}_{-4.2}$	1.02
$1.00 : 1.25$	2.00	5.8	$^{+5.3}_{-5.1}$	1.01
$1.25 : 1.50$	1.84	7.7	$^{+7.4}_{-5.6}$	1.01

Table 2: *Differential cross section of $D^{*\pm}$ production in η^{D^*}. See Table 1 for other details.*

z^{D^*}	$\frac{d\sigma}{dz^{D^*}}$ (nb)	δ_{stat} (%)	δ_{syst} (%)	C_r
$0.000 : 0.100$	3.02	12	$^{+8.6}_{-7.1}$	1.00
$0.100 : 0.200$	6.83	6.1	$^{+6.1}_{-5.0}$	1.01
$0.200 : 0.325$	8.18	3.5	$^{+5.5}_{-4.9}$	1.02
$0.325 : 0.450$	9.20	2.5	$^{+4.6}_{-3.8}$	1.03
$0.450 : 0.575$	9.14	2.3	$^{+4.6}_{-4.0}$	1.05
$0.575 : 0.800$	5.12	2.4	$^{+6.5}_{-5.1}$	1.07
$0.800 : 1.000$	0.063	9.1	$^{+9.9}_{-8.5}$	1.07

Table 3: *Differential cross section of $D^{*\pm}$ production in z^{D^*}. See Table 1 for other details.*

Q^2 (GeV^2)	$\frac{d\sigma}{dQ^2}$ (nb/ GeV^2)	δ_{stat} (%)	δ_{syst} (%)	C_r
5.0 : 8.0	0.499	3.9	$^{+6.7}_{-6.1}$	1.03
8.0 : 10.0	0.307	4.3	$^{+6.0}_{-5.2}$	1.03
10.0 : 13.0	0.222	4.0	$^{+4.9}_{-4.1}$	1.02
13.0 : 19.0	0.125	3.5	$^{+5.6}_{-5.0}$	1.03
19.0 : 27.5	0.752×10^{-1}	3.7	$^{+4.9}_{-4.0}$	1.04
27.5 : 40.0	0.415×10^{-1}	3.9	$^{+4.8}_{-3.8}$	1.04
40.0 : 60.0	0.169×10^{-1}	4.7	$^{+5.6}_{-5.6}$	1.05
60.0 : 100.0	0.747×10^{-2}	5.0	$^{+7.1}_{-5.1}$	1.06
100.0 : 200.0	0.171×10^{-2}	7.8	$^{+6.6}_{-4.4}$	1.07
200.0 : 1000.0	0.140×10^{-3}	13	$^{+6.1}_{-5.2}$	1.14

Table 4: *Differential cross section of $D^{*\pm}$ production in Q^2. See Table 1 for other details.*

y	$\frac{d\sigma}{dy}$ (nb)	δ_{stat} (%)	δ_{syst} (%)	C_r
0.02 : 0.05	1.20×10^1	7.9	$^{+16}_{-12}$	1.07
0.05 : 0.09	2.07×10^1	3.4	$^{+6.7}_{-6.5}$	1.05
0.09 : 0.13	1.79×10^1	3.4	$^{+4.5}_{-4.0}$	1.04
0.13 : 0.18	1.37×10^1	3.6	$^{+4.6}_{-4.8}$	1.04
0.18 : 0.26	1.13×10^1	3.3	$^{+4.8}_{-3.7}$	1.04
0.26 : 0.36	8.03	3.7	$^{+4.8}_{-4.0}$	1.03
0.36 : 0.50	5.09	4.2	$^{+5.2}_{-4.5}$	1.02
0.50 : 0.70	2.90	6.0	$^{+9.3}_{-7.1}$	1.01

Table 5: *Differential cross section of $D^{*\pm}$ production in y. See Table 1 for other details.*

x	$\frac{d\sigma}{dx}$ (nb)	δ_{stat} (%)	δ_{syst} (%)	C_r
$(0.8 : 4.0) \times 10^{-4}$	0.475×10^4	3.5	$^{+6.0}_{-5.3}$	1.06
$(0.4 : 1.6) \times 10^{-3}$	0.198×10^4	2.1	$^{+4.8}_{-3.9}$	1.03
$(1.6 : 5.0) \times 10^{-3}$	0.357×10^3	2.6	$^{+4.9}_{-3.9}$	1.02
$(0.5 : 1.0) \times 10^{-2}$	0.553×10^2	5.7	$^{+6.3}_{-5.1}$	0.99
$(0.1 : 1.0) \times 10^{-1}$	0.159×10^1	10.7	$^{+9.2}_{-8.4}$	1.08

Table 6: *Differential cross section of $D^{*\pm}$ production in x. See Table 1 for other details.*

Q^2 (GeV^2)	y	σ_{vis} (pb)	δ_{stat} (%)	δ_{syst} (%)	$\sigma_{\text{vis}}^{\text{beauty}}$ (pb)	C_r
	0.020 : 0.050	120	23	$^{+19}_{-20}$	0.0	1.04
	0.050 : 0.090	279	10	$^{+11}_{-11}$	1.5	1.04
5 : 9	0.090 : 0.160	421	6.0	$^{+6.8}_{-7.0}$	5.2	1.04
	0.160 : 0.320	550	5.3	$^{+6.5}_{-5.8}$	11.0	1.03
	0.320 : 0.700	456	6.8	$^{+6.3}_{-5.5}$	18.2	1.02
	0.020 : 0.050	108	14	$^{+17}_{-12}$	0.1	1.05
	0.050 : 0.090	178	6.5	$^{+7.0}_{-6.0}$	1.2	1.04
9 : 14	0.090 : 0.160	220	5.8	$^{+4.7}_{-4.6}$	2.9	1.03
	0.160 : 0.320	352	5.1	$^{+4.5}_{-3.7}$	8.1	1.02
	0.320 : 0.700	307	7.2	$^{+6.6}_{-5.0}$	12.5	1.00
	0.020 : 0.050	65.1	15	$^{+16}_{-12}$	0.2	1.07
	0.050 : 0.090	160	6.4	$^{+6.2}_{-7.2}$	1.2	1.04
14 : 23	0.090 : 0.160	205	5.6	$^{+4.7}_{-4.7}$	3.1	1.03
	0.160 : 0.320	267	5.9	$^{+4.9}_{-4.4}$	9.0	1.03
	0.320 : 0.700	250	7.4	$^{+5.7}_{-6.7}$	13.5	1.01
	0.020 : 0.050	37.1	29	$^{+18}_{-18}$	0.1	1.08
	0.050 : 0.090	134	7.0	$^{+7.5}_{-7.8}$	0.9	1.06
23 : 45	0.090 : 0.160	196	5.3	$^{+4.4}_{-4.3}$	3.6	1.05
	0.160 : 0.320	275	5.1	$^{+4.1}_{-3.4}$	10.2	1.03
	0.320 : 0.700	284	6.1	$^{+6.4}_{-4.5}$	14.7	1.02
	0.020 : 0.050	14.2	38	$^{+35}_{-18}$	0.0	1.25
	0.050 : 0.090	72.1	9.6	$^{+8.0}_{-7.2}$	1.2	1.07
45 : 100	0.090 : 0.160	87.0	8.4	$^{+4.9}_{-4.6}$	3.9	1.04
	0.160 : 0.320	182	5.7	$^{+5.3}_{-3.9}$	9.4	1.04
	0.320 : 0.700	175	7.6	$^{+6.6}_{-5.6}$	14.0	1.02
	0.020 : 0.350	80.2	11	$^{+7.6}_{-4.2}$	5.8	1.1
100 : 158	0.350 : 0.700	45.1	16	$^{+7.6}_{-7.8}$	5.0	0.99
	0.020 : 0.300	59.8	14	$^{+4.8}_{-6.3}$	3.5	1.16
158 : 251	0.300 : 0.700	37.3	17	$^{+6.6}_{-4.9}$	4.3	1.04
	0.020 : 0.275	28.4	24	$^{+8.2}_{-10}$	2.4	1.26
251 : 1000	0.275 : 0.700	46.7	21	$^{+8.7}_{-5.1}$	6.9	1.07

Table 7: *Visible cross sections, σ_{vis}, for $D^{*\pm}$ production in bins of Q^2 and y. The second but last column reports the estimated contribution from beauty decays, based on the* RAPGAP *beauty MC rescaled to ZEUS data. See Table 1 for other details.*

Q^2 (GeV^2)	y	δ_1 (%)	δ_2 (%)	δ_3 (%)	δ_4 (%)	δ_5 (%)	δ_6 (%)	δ_7 (%)	δ_9 (%)	δ_{11} (%)	δ_{12} (%)	δ_{13} (%)	δ_{14} (%)	δ_{15} (%)	δ_{16} (%)	δ_{17} (%)
5 : 9	0.020 : 0.050	$^{+11}_{-12}$	$^{+1.8}_{+0.6}$	$^{+7.4}_{-2.7}$	$^{+9.0}_{-9.0}$	-7.0	-3.4	$^{+2.5}_{-2.4}$	$^{+2.5}_{-2.5}$	$^{+8.8}_{-8.8}$	$^{+0.0}_{-0.0}$	$^{+0.0}_{+0.0}$	$^{-4.2}_{+4.2}$	+1.8	$^{+0.1}_{-0.1}$	+2.2
	0.050 : 0.090	$^{+3.5}_{-4.0}$	$^{+5.1}_{-4.8}$	$^{+2.3}_{-3.0}$	$^{+6.6}_{-6.6}$	+0.7	-1.9	$^{+2.4}_{-2.2}$	$^{+2.1}_{-2.1}$	$^{+3.4}_{-3.4}$	$^{-0.1}_{+0.1}$	$^{+0.0}_{+0.0}$	$^{-1.9}_{+2.3}$	+3.0	$^{-0.7}_{+0.8}$	-1.6
	0.090 : 0.160	$^{+1.5}_{-3.4}$	$^{+3.3}_{-4.0}$	$^{+2.6}_{-1.5}$	$^{+1.1}_{-1.1}$	+1.0	+0.5	$^{+2.3}_{-2.2}$	$^{+1.8}_{-1.8}$	$^{+2.3}_{-2.3}$	$^{+0.1}_{-0.1}$	$^{+0.0}_{+0.0}$	$^{+0.6}_{-0.8}$	+1.8	$^{-1.4}_{+1.5}$	-2.0
	0.160 : 0.320	$^{+0.9}_{+0.1}$	$^{+2.9}_{-2.7}$	$^{+1.1}_{-0.8}$	$^{+3.5}_{-3.5}$	+0.6	+0.3	$^{+2.2}_{-2.1}$	$^{+1.8}_{-1.8}$	$^{+1.6}_{-1.6}$	$^{-0.0}_{-0.0}$	$^{+0.3}_{-0.5}$	$^{+0.7}_{-0.9}$	-0.5	$^{-1.7}_{+1.8}$	+0.7
	0.320 : 0.700	$^{-1.5}_{+1.7}$	$^{+1.9}_{-0.7}$	$^{+0.5}_{-0.6}$	$^{+1.9}_{-1.9}$	+0.2	-1.5	$^{+2.0}_{-1.9}$	$^{+1.9}_{-1.9}$	$^{+1.7}_{-1.7}$	$^{-0.0}_{-0.0}$	$^{+1.4}_{-2.8}$	$^{+0.3}_{-0.4}$	-0.6	$^{-1.4}_{+1.5}$	+3.1
9 : 14	0.020 : 0.050	$^{+11}_{-6.9}$	$^{-4.8}_{+7.3}$	$^{+1.5}_{-2.5}$	$^{-2.5}_{+2.5}$	-0.1	-2.1	$^{+2.2}_{-2.1}$	$^{+2.4}_{-2.4}$	$^{+6.1}_{-6.1}$	$^{+0.1}_{-0.1}$	$^{+0.0}_{+0.0}$	$^{-4.5}_{+4.7}$	+3.0	$^{-0.7}_{+0.7}$	+1.4
	0.050 : 0.090	$^{+3.1}_{-3.2}$	$^{+0.2}_{+1.9}$	$^{+1.0}_{-1.3}$	$^{+2.1}_{-2.1}$	+0.6	+0.1	$^{+2.2}_{-2.1}$	$^{+2.0}_{-2.0}$	$^{+2.4}_{-2.4}$	$^{+0.0}_{-0.0}$	$^{+0.0}_{-0.0}$	$^{-1.2}_{+1.5}$	+2.7	$^{-1.2}_{+1.2}$	-1.6
	0.090 : 0.160	$^{+0.5}_{-0.6}$	$^{-0.1}_{+0.3}$	$^{+1.2}_{-0.6}$	$^{+1.6}_{-1.6}$	+0.5	-0.3	$^{+2.1}_{-2.0}$	$^{+1.7}_{-1.7}$	$^{+1.7}_{-1.7}$	$^{-0.2}_{+0.2}$	$^{-0.0}_{+0.0}$	$^{-0.1}_{+0.1}$	+0.8	$^{-1.6}_{+1.7}$	-2.0
	0.160 : 0.320	$^{+0.0}_{+0.5}$	$^{+0.2}_{+0.5}$	$^{+0.3}_{-0.7}$	$^{-0.5}_{+0.5}$	+0.3	+0.5	$^{+2.1}_{-2.0}$	$^{+1.8}_{-1.8}$	$^{+1.5}_{-1.5}$	$^{-0.1}_{+0.1}$	$^{+0.1}_{-0.1}$	$^{+0.6}_{-0.7}$	+1.1	$^{-1.8}_{+1.9}$	+0.4
	0.320 : 0.700	$^{-2.8}_{+3.8}$	$^{+1.1}_{-0.7}$	$^{+0.1}_{-0.1}$	$^{-0.4}_{+0.4}$	+0.4	-0.2	$^{+1.9}_{-1.9}$	$^{+1.8}_{-1.8}$	$^{+1.9}_{-1.9}$	$^{+0.2}_{-0.3}$	$^{+0.8}_{-1.6}$	$^{+0.4}_{-0.5}$	+0.2	$^{-1.8}_{+2.0}$	+2.8
14 : 23	0.020 : 0.050	$^{+12}_{-8.8}$	$^{-3.8}_{+6.4}$	$^{+0.4}_{-0.2}$	$^{-0.0}_{+0.0}$	+0.3	+2.5	$^{+2.1}_{-2.0}$	$^{+2.4}_{-2.4}$	$^{+6.0}_{-6.0}$	$^{+0.2}_{-0.2}$	$^{+0.0}_{+0.0}$	$^{-2.7}_{+2.4}$	+4.1	$^{-0.8}_{+0.8}$	+1.7
	0.050 : 0.090	$^{+2.5}_{-3.9}$	$^{-3.8}_{+1.5}$	$^{+0.3}_{-0.3}$	$^{-0.9}_{+0.9}$	+0.2	+1.0	$^{+2.1}_{-2.0}$	$^{+2.0}_{-2.0}$	$^{+2.3}_{-2.3}$	$^{+0.1}_{-0.1}$	$^{+0.0}_{+0.0}$	$^{-0.9}_{+1.1}$	+2.3	$^{-1.9}_{+1.8}$	-1.7
	0.090 : 0.160	$^{+1.3}_{+0.4}$	$^{-0.4}_{+0.8}$	$^{+0.2}_{-0.3}$	$^{+0.3}_{+0.3}$	-1.0	-1.6	$^{+2.0}_{-1.9}$	$^{+1.7}_{-1.7}$	$^{+1.6}_{-1.6}$	$^{-0.1}_{+0.1}$	$^{+0.0}_{-0.0}$	$^{+0.3}_{-0.4}$	+0.7	$^{-2.3}_{+2.2}$	-2.0
	0.160 : 0.320	$^{-0.9}_{+0.5}$	$^{-0.6}_{-0.2}$	$^{+0.0}_{-0.0}$	$^{+0.6}_{-0.6}$	-0.9	+1.7	$^{+1.9}_{-1.9}$	$^{+1.7}_{-1.7}$	$^{+1.4}_{-1.4}$	$^{+0.1}_{-0.2}$	$^{+0.2}_{-0.3}$	$^{+1.0}_{-1.3}$	+0.4	$^{-2.6}_{+2.6}$	+0.4
	0.320 : 0.700	$^{-2.9}_{+1.3}$	$^{-0.3}_{-1.7}$	$^{+0.0}_{-0.0}$	$^{+0.1}_{-0.1}$	-0.3	-3.1	$^{+1.9}_{-1.8}$	$^{+1.8}_{-1.8}$	$^{+1.8}_{-1.8}$	$^{+0.2}_{-0.3}$	$^{+1.0}_{-1.9}$	$^{+0.3}_{-0.4}$	-1.5	$^{-2.7}_{+2.7}$	+2.9
23 : 45	0.020 : 0.050	$^{+9.5}_{-8.4}$	$^{-6.7}_{+12}$	$^{+0.0}_{-0.0}$	$^{-0.0}_{+0.0}$	+1.3	-13	$^{+1.9}_{-1.8}$	$^{+2.2}_{-2.2}$	$^{+7.0}_{-7.0}$	$^{-0.3}_{+0.3}$	$^{+0.0}_{+0.0}$	$^{-2.3}_{+2.4}$	+3.7	$^{-0.6}_{+0.6}$	+1.7
	0.050 : 0.090	$^{+4.3}_{-4.6}$	$^{-4.8}_{+4.3}$	$^{+0.0}_{-0.0}$	$^{-0.0}_{+0.0}$	-0.3	-0.2	$^{+1.8}_{-1.7}$	$^{+1.9}_{-1.9}$	$^{+2.3}_{-2.3}$	$^{+0.0}_{-0.0}$	$^{+0.0}_{+0.0}$	$^{-0.4}_{+0.5}$	+0.1	$^{-1.5}_{+1.6}$	-1.4
	0.090 : 0.160	$^{+0.9}_{-1.1}$	$^{-1.4}_{+1.8}$	$^{+0.0}_{-0.0}$	$^{-0.0}_{+0.0}$	+0.3	-0.1	$^{+1.8}_{-1.7}$	$^{+1.6}_{-1.6}$	$^{+1.5}_{-1.5}$	$^{+0.2}_{-0.3}$	$^{-0.0}_{+0.0}$	$^{-0.3}_{+0.3}$	+0.0	$^{-1.7}_{+1.7}$	-2.1
	0.160 : 0.320	$^{-1.0}_{+1.2}$	$^{-0.3}_{-0.4}$	$^{+0.0}_{-0.0}$	$^{-0.0}_{+0.0}$	+0.2	+0.1	$^{+1.8}_{-1.7}$	$^{+1.6}_{-1.6}$	$^{+1.3}_{-1.3}$	$^{+0.1}_{-0.2}$	$^{+0.1}_{-0.2}$	$^{+0.0}_{-0.1}$	+0.7	$^{-1.8}_{+1.8}$	+0.4
	0.320 : 0.700	$^{-2.6}_{+3.5}$	$^{+0.0}_{+1.1}$	$^{+0.0}_{-0.0}$	$^{-0.0}_{+0.0}$	+1.0	+0.0	$^{+1.8}_{-1.7}$	$^{+1.8}_{-1.8}$	$^{+1.5}_{-1.5}$	$^{-0.2}_{+0.1}$	$^{+0.6}_{-1.3}$	$^{+0.2}_{-0.2}$	+2.1	$^{-1.7}_{+1.7}$	+2.4
45 : 100	0.020 : 0.050	$^{+26}_{-6.4}$	$^{-9.7}_{+18}$	$^{+0.0}_{-0.0}$	$^{-0.0}_{+0.0}$	-0.1	+2.3	$^{+1.5}_{-1.4}$	$^{+2.0}_{-2.0}$	$^{+13}_{-13}$	$^{+0.0}_{-0.0}$	$^{+0.0}_{+0.0}$	$^{-2.6}_{+3.4}$	+5.0	$^{-2.2}_{+2.0}$	+3.5
	0.050 : 0.090	$^{+4.2}_{-3.5}$	$^{-4.0}_{+3.7}$	$^{+0.0}_{-0.0}$	$^{-0.0}_{+0.0}$	-2.0	-0.1	$^{+1.5}_{-1.5}$	$^{+1.8}_{-1.8}$	$^{+3.1}_{-3.1}$	$^{+0.1}_{-0.1}$	$^{+0.0}_{+0.0}$	$^{-0.2}_{+0.0}$	+3.3	$^{-1.4}_{+1.3}$	-1.6
	0.090 : 0.160	$^{+1.1}_{-0.7}$	$^{-2.0}_{+2.4}$	$^{+0.0}_{-0.0}$	$^{-0.0}_{+0.0}$	-0.8	-0.3	$^{+1.5}_{-1.4}$	$^{+1.5}_{-1.5}$	$^{+1.7}_{-1.7}$	$^{+0.3}_{-0.4}$	$^{+0.0}_{-0.0}$	$^{-0.0}_{+0.0}$	+1.5	$^{-1.9}_{+1.7}$	-2.1
	0.160 : 0.320	$^{-0.7}_{-0.1}$	$^{-1.5}_{+1.9}$	$^{+0.0}_{-0.0}$	$^{-0.0}_{+0.0}$	+0.3	+0.5	$^{+1.6}_{-1.5}$	$^{+1.5}_{-1.5}$	$^{+1.4}_{-1.4}$	$^{+0.6}_{-0.7}$	$^{+0.0}_{-0.0}$	$^{-0.0}_{-0.0}$	+3.0	$^{-2.3}_{+2.1}$	+0.2
	0.320 : 0.700	$^{-2.8}_{+3.2}$	$^{-0.8}_{-0.3}$	$^{+0.0}_{-0.0}$	$^{-0.0}_{+0.0}$	-0.6	-2.4	$^{+1.7}_{-1.6}$	$^{+1.6}_{-1.6}$	$^{+1.6}_{-1.6}$	$^{+0.5}_{-0.7}$	$^{+0.4}_{-0.9}$	$^{-0.6}_{+0.7}$	+2.4	$^{-2.7}_{+2.5}$	+2.9
100 : 158	0.020 : 0.350	$^{+1.7}_{-0.6}$	$^{-1.3}_{+4.4}$	$^{+0.0}_{-0.0}$	$^{-0.0}_{+0.0}$	-2.2	+4.4	$^{+1.3}_{-1.3}$	$^{+1.4}_{-1.4}$	$^{+1.8}_{-1.8}$	$^{+0.9}_{-1.1}$	$^{+0.0}_{-0.0}$	$^{-0.2}_{+0.2}$	+1.3	$^{-1.3}_{+1.2}$	-0.2
	0.350 : 0.700	$^{-5.3}_{+0.8}$	$^{-2.5}_{-0.9}$	$^{+0.0}_{-0.0}$	$^{-0.0}_{+0.0}$	+1.8	+4.4	$^{+1.4}_{-1.4}$	$^{+1.5}_{-1.5}$	$^{+2.9}_{-2.9}$	$^{+2.6}_{-3.2}$	$^{+0.5}_{-1.1}$	$^{+0.1}_{-0.4}$	-0.2	$^{-1.3}_{+1.1}$	+2.9
158 : 251	0.020 : 0.300	$^{+0.3}_{-0.8}$	$^{-4.3}_{+2.0}$	$^{+0.0}_{-0.0}$	$^{-0.0}_{+0.0}$	-1.9	-0.3	$^{+1.2}_{-1.2}$	$^{+1.3}_{-1.3}$	$^{+3.0}_{-3.0}$	$^{+0.8}_{-1.0}$	$^{+0.1}_{-0.1}$	$^{+0.4}_{-0.6}$	-1.3	$^{-0.9}_{+0.8}$	+0.1
	0.300 : 0.700	$^{-2.6}_{+2.6}$	$^{-0.2}_{+0.6}$	$^{+0.0}_{-0.0}$	$^{-0.0}_{+0.0}$	+1.8	+1.7	$^{+1.4}_{-1.3}$	$^{+1.4}_{-1.4}$	$^{+3.0}_{-3.0}$	$^{+0.1}_{-0.7}$	$^{+0.5}_{-1.0}$	$^{+0.3}_{-0.5}$	+1.1	$^{-1.0}_{+0.9}$	+3.0
251 : 1000	0.020 : 0.275	$^{-0.6}_{-2.2}$	$^{-5.8}_{+5.9}$	$^{+0.0}_{-0.0}$	$^{-0.0}_{+0.0}$	-4.6	-0.0	$^{+1.2}_{-1.2}$	$^{+1.3}_{-1.3}$	$^{+4.6}_{-4.6}$	$^{+0.8}_{-1.3}$	$^{+0.0}_{+0.0}$	$^{-1.0}_{+0.9}$	-3.3	$^{+0.1}_{-0.1}$	-0.3
	0.275 : 0.700	$^{-0.8}_{+4.3}$	$^{-1.7}_{+3.8}$	$^{+0.0}_{-0.0}$	$^{-0.0}_{+0.0}$	+2.5	+3.5	$^{+1.4}_{-1.3}$	$^{+1.4}_{-1.4}$	$^{+3.6}_{-3.6}$	$^{-0.1}_{-0.1}$	$^{+0.7}_{-1.4}$	$^{-0.5}_{+0.4}$	-1.4	$^{-1.0}_{+0.9}$	+0.9

Table 8: *Individual systematical uncertainties as defined in Section 7 for the double-differential cross sections in bins of Q^2 and y. The uncertainty δ_8 and δ_{10} are not reported as δ_8 is constant ($+2\%$) and δ_{10} was found to be negligible. The overall normalisation uncertanties $\delta_{18} = \pm 1.9\%$ and $\delta_{19} = \pm 1.5\%$ are also not listed.*

Q^2 (GeV²)	x	δ_{m_c} (%)	δ_μ (%)	δ_{α_s} (%)	δ_{α_K} (%)	δ_{k_T} (%)	$\delta_{\rm b}$ (%)
	0.00160	$^{+8.3}_{-5.6}$	$^{-6.5}_{+14}$	$^{+0.6}_{+0.2}$	$^{-4.5}_{+7.5}$	$^{-0.2}_{+0.6}$	±0.0
	0.00080	$^{+0.3}_{+1.0}$	$^{-3.9}_{+7.8}$	$^{-0.3}_{+0.6}$	$^{-3.5}_{+6.1}$	$^{-1.3}_{+1.3}$	±0.3
7	0.00050	$^{-1.3}_{+2.0}$	$^{-3.2}_{+5.0}$	$^{+0.1}_{+0.8}$	$^{-2.9}_{+6.5}$	$^{-1.3}_{+1.8}$	±0.6
	0.00030	$^{-3.2}_{+3.3}$	$^{-1.4}_{+0.2}$	$^{-0.9}_{+1.2}$	$^{-2.6}_{+5.9}$	$^{-2.5}_{+2.2}$	±1.0
	0.00013	$^{-3.7}_{+5.7}$	$^{+4.7}_{-6.3}$	$^{-1.6}_{+2.5}$	$^{-2.4}_{+5.9}$	$^{-4.0}_{+4.2}$	±2.2
	0.00300	$^{+9.5}_{-6.2}$	$^{-6.5}_{+15}$	$^{+1.4}_{+0.0}$	$^{-3.6}_{+8.0}$	$^{+1.6}_{+0.1}$	±0.0
	0.00150	$^{+0.1}_{-1.1}$	$^{-5.4}_{+7.8}$	$^{-0.1}_{-0.6}$	$^{-3.3}_{+5.3}$	$^{-0.7}_{-0.1}$	±0.3
12	0.00080	$^{-0.6}_{+0.8}$	$^{-3.8}_{+5.7}$	$^{-0.1}_{+0.1}$	$^{-2.5}_{+5.5}$	$^{-0.9}_{+1.0}$	±0.7
	0.00050	$^{-2.5}_{+2.2}$	$^{-2.5}_{+2.0}$	$^{-0.5}_{+0.0}$	$^{-2.4}_{+5.0}$	$^{-1.9}_{+1.2}$	±1.2
	0.00022	$^{-3.2}_{+3.9}$	$^{+3.1}_{-4.4}$	$^{-1.6}_{+1.7}$	$^{-2.2}_{+5.4}$	$^{-3.1}_{+1.8}$	±2.2
	0.00450	$^{+8.8}_{-6.1}$	$^{-6.5}_{+13}$	$^{+0.9}_{+0.7}$	$^{-3.2}_{+6.2}$	$^{+1.1}_{-1.0}$	±0.1
	0.00250	$^{+0.3}_{-0.9}$	$^{-5.7}_{+7.0}$	$^{+0.4}_{-0.6}$	$^{-3.2}_{+3.7}$	$^{-0.3}_{-0.6}$	±0.4
18	0.00135	$^{-0.4}_{+0.8}$	$^{-4.4}_{+6.1}$	$^{+0.6}_{+0.1}$	$^{-2.4}_{+4.8}$	$^{-0.5}_{+0.6}$	±0.8
	0.00080	$^{-1.5}_{+1.0}$	$^{-4.0}_{+3.2}$	$^{+0.3}_{+0.3}$	$^{-1.9}_{+4.4}$	$^{-0.9}_{+0.7}$	±1.8
	0.00035	$^{-3.0}_{+2.7}$	$^{+1.8}_{-3.7}$	$^{-1.0}_{+1.0}$	$^{-2.5}_{+4.5}$	$^{-2.9}_{+1.4}$	±3.0
	0.00800	$^{+8.4}_{-7.3}$	$^{-7.0}_{+11}$	$^{+0.6}_{-0.5}$	$^{-3.5}_{+5.1}$	$^{+0.3}_{-1.7}$	±0.1
	0.00550	$^{+1.3}_{-0.0}$	$^{-5.8}_{+8.4}$	$^{+0.5}_{-0.3}$	$^{-1.9}_{+3.2}$	$^{+0.3}_{-0.3}$	±0.3
32	0.00240	$^{+0.5}_{+0.5}$	$^{-3.6}_{+6.4}$	$^{-0.1}_{+0.3}$	$^{-1.7}_{+3.9}$	$^{-0.2}_{+0.0}$	±0.9
	0.00140	$^{-0.5}_{+1.3}$	$^{-3.5}_{+4.6}$	$^{+0.2}_{+0.1}$	$^{-1.6}_{+3.9}$	$^{-0.4}_{+0.6}$	±2.0
	0.00080	$^{-2.9}_{+3.0}$	$^{-0.4}_{-1.6}$	$^{-0.8}_{+0.5}$	$^{-2.2}_{+3.6}$	$^{-2.2}_{+1.1}$	±2.9
	0.01500	$^{+9.3}_{-6.5}$	$^{-5.2}_{+10}$	$^{+0.6}_{+0.4}$	$^{-1.8}_{+6.2}$	$^{+1.6}_{+0.4}$	±0.0
	0.00800	$^{+0.6}_{-1.7}$	$^{-4.8}_{+6.0}$	$^{-0.3}_{-0.7}$	$^{-1.9}_{+2.3}$	$^{-0.1}_{-0.6}$	±0.9
60	0.00500	$^{-0.2}_{+0.8}$	$^{-3.9}_{+5.2}$	$^{+0.1}_{-0.0}$	$^{-1.4}_{+2.7}$	$^{-0.3}_{+0.3}$	±2.4
	0.00320	$^{-0.9}_{+1.4}$	$^{-3.7}_{+5.0}$	$^{-0.1}_{-0.2}$	$^{-1.6}_{+2.8}$	$^{-0.4}_{+0.0}$	±2.9
	0.00140	$^{-2.4}_{+1.8}$	$^{-1.5}_{+1.3}$	$^{-0.1}_{-0.0}$	$^{-1.8}_{+2.8}$	$^{-1.3}_{+0.6}$	±4.8
	0.01000	$^{+0.2}_{+0.8}$	$^{-4.6}_{+5.3}$	$^{+0.4}_{+0.1}$	$^{-1.5}_{+2.3}$	$^{+0.0}_{+0.3}$	±4.2
120	0.00200	$^{-0.8}_{+1.3}$	$^{-2.0}_{+2.3}$	$^{+0.4}_{-0.5}$	$^{-1.3}_{+1.9}$	$^{-1.0}_{+0.8}$	±7.2
	0.01300	$^{-0.1}_{-0.1}$	$^{-3.7}_{+3.8}$	$^{+0.4}_{-0.1}$	$^{-0.9}_{+1.4}$	$^{+0.1}_{+0.0}$	±4.1
200	0.00500	$^{-1.9}_{+1.3}$	$^{-3.8}_{+3.8}$	$^{-0.3}_{-0.6}$	$^{-1.5}_{+1.2}$	$^{-0.1}_{+0.1}$	±7.5
	0.02500	$^{-0.5}_{+0.4}$	$^{-3.8}_{+3.4}$	$^{-0.4}_{-0.0}$	$^{-0.7}_{+1.2}$	$^{+0.4}_{-0.4}$	±5.1
350	0.01000	$^{-0.2}_{+1.3}$	$^{-2.8}_{+3.7}$	$^{+0.0}_{+0.3}$	$^{-0.6}_{+0.9}$	$^{+0.0}_{+0.1}$	±10.6

Table 9: *Breakdown of the theoretical uncertainty on $\sigma^{c\bar{c}}_{\rm red}(x,Q^2)$, showing the uncertainty from the variation of charm mass (δ_{m_c}), of the renormalisation and factorisation scales (δ_μ), of α_S (δ_{α_s}), of the fragmentation function (δ_{α_K}), of the transverse fragmentation (δ_{k_T}), and of the expected beauty component ($\delta_{\rm b}$). The upper (lower) value gives the effect of a positive (negative) variation of the parameter.*

Q^2 (GeV^2)	x	$\sigma_{\mathrm{red}}^{c\bar{c}}$	$\delta_{\mathrm{stat.}}$ (%)	$\delta_{\mathrm{syst.}}$ (%)	$\delta_{\mathrm{theo.}}$ (%)	$\mathcal{A}_{ps}$ (%)
	0.00160	0.057	23	$+19$ -20	$+18$ -9.7	0.227
	0.00080	0.124	10	$+11$ -11	$+10$ -5.4	0.377
7	0.00050	0.164	6.2	$+6.8$ -7.1	$+8.7$ -4.7	0.440
	0.00030	0.187	5.5	$+6.7$ -6.0	$+7.3$ -5.2	0.440
	0.00013	0.248	7.4	$+6.6$ -5.7	$+11$ -9.0	0.299
	0.00300	0.098	14	$+17$ -12	$+19$ -9.7	0.256
	0.00150	0.152	6.6	$+7.1$ -6.0	$+9.4$ -6.5	0.423
12	0.00080	0.175	6.0	$+4.7$ -4.6	$+8.1$ -4.7	0.490
	0.00050	0.239	5.4	$+4.6$ -3.8	$+6.0$ -4.9	0.492
	0.00022	0.335	7.8	$+6.9$ -5.3	$+8.1$ -7.2	0.332
	0.00450	0.081	15	$+16$ -12	$+17$ -9.5	0.262
	0.00250	0.168	6.5	$+6.2$ -7.2	$+8.0$ -6.7	0.456
18	0.00135	0.199	5.8	$+4.7$ -4.8	$+7.9$ -5.1	0.529
	0.00080	0.216	6.3	$+5.1$ -4.6	$+5.9$ -5.0	0.544
	0.00035	0.324	8.3	$+6.1$ -7.1	$+6.5$ -6.8	0.370
	0.00800	0.068	29	$+18$ -19	$+15$ -11	0.236
	0.00550	0.159	7.1	$+7.5$ -7.9	$+9.1$ -6.2	0.478
32	0.00240	0.234	5.5	$+4.5$ -4.4	$+7.6$ -4.1	0.560
	0.00140	0.266	5.5	$+4.3$ -3.6	$+6.5$ -4.4	0.594
	0.00080	0.390	6.8	$+6.8$ -4.7	$+5.7$ -5.5	0.430
	0.01500	0.068	38	$+35$ -18	$+15$ -8.6	0.166
	0.00800	0.173	9.9	$+8.1$ -7.3	$+6.6$ -5.6	0.465
60	0.00500	0.161	9.2	$+5.2$ -4.9	$+6.4$ -4.8	0.570
	0.00320	0.258	6.4	$+5.6$ -4.1	$+6.6$ -5.1	0.624
	0.00140	0.327	9.0	$+7.2$ -6.2	$+6.0$ -6.0	0.516
	0.01000	0.130	12	$+8.2$ -4.6	$+7.2$ -6.4	0.491
120	0.00200	0.287	21	$+8.7$ -8.9	$+7.9$ -7.7	0.583
	0.01300	0.176	17	$+5.2$ -6.8	$+5.8$ -5.6	0.465
200	0.00500	0.239	22	$+7.6$ -5.6	$+8.6$ -8.8	0.624
	0.02500	0.103	29	$+9.0$ -11	$+6.2$ -6.4	0.433
350	0.01000	0.193	29	$+11$ -6.2	$+11$ -11	0.636

Table 10: *The reduced cross-section $\sigma_{\mathrm{red}}^{c\bar{c}}(x, Q^2)$ with statistical, systematic and theoretical uncertainties. The last column shows the kinematical acceptance.*
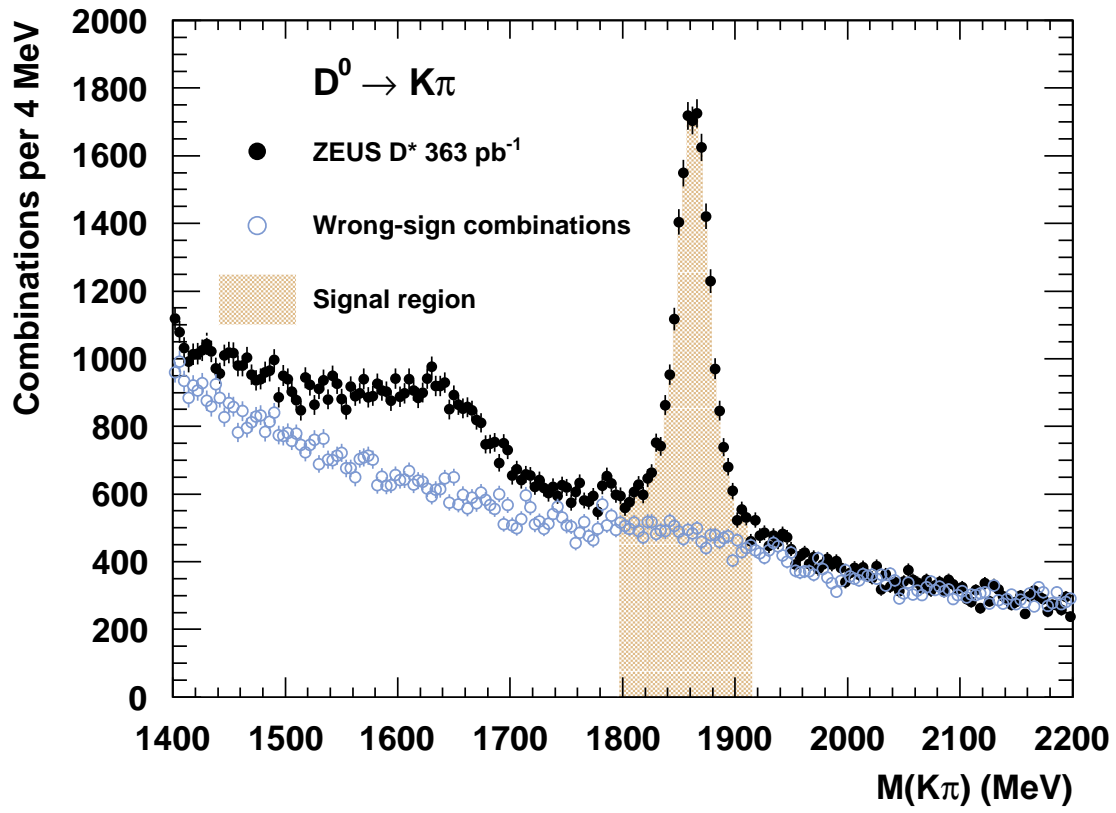
23

Figure 1: *Distribution of $M(K\pi)$ for $D^{*\pm}$ candidates with $143.2 < \Delta M < 147.7$ MeV (filled circles) and for wrong-sign combinations (empty circles). The D^0 signal region is marked as a shaded area.*
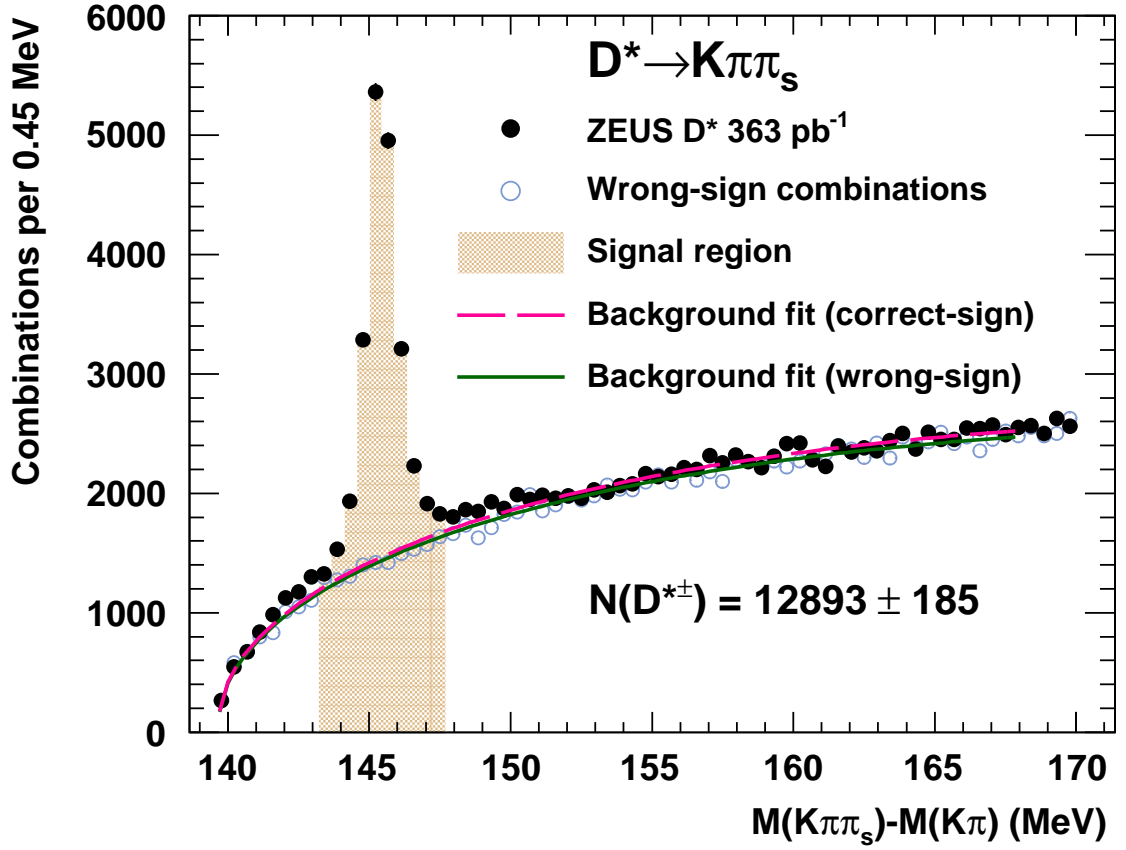
Figure 2: *Distribution of the mass difference, $\Delta M = M(K\pi\pi_s) - M(K\pi)$, for the $D^{*\pm}$ candidates with $1.80 < M(K\pi) < 1.92$ GeV (filled circles) and for wrong-sign combinations (empty circles). The background fit described in the text is shown as a dashed (continuous) line for correct-sign (wrong-sign) combinations. The $D^{*\pm}$ signal region is marked as a shaded area.*
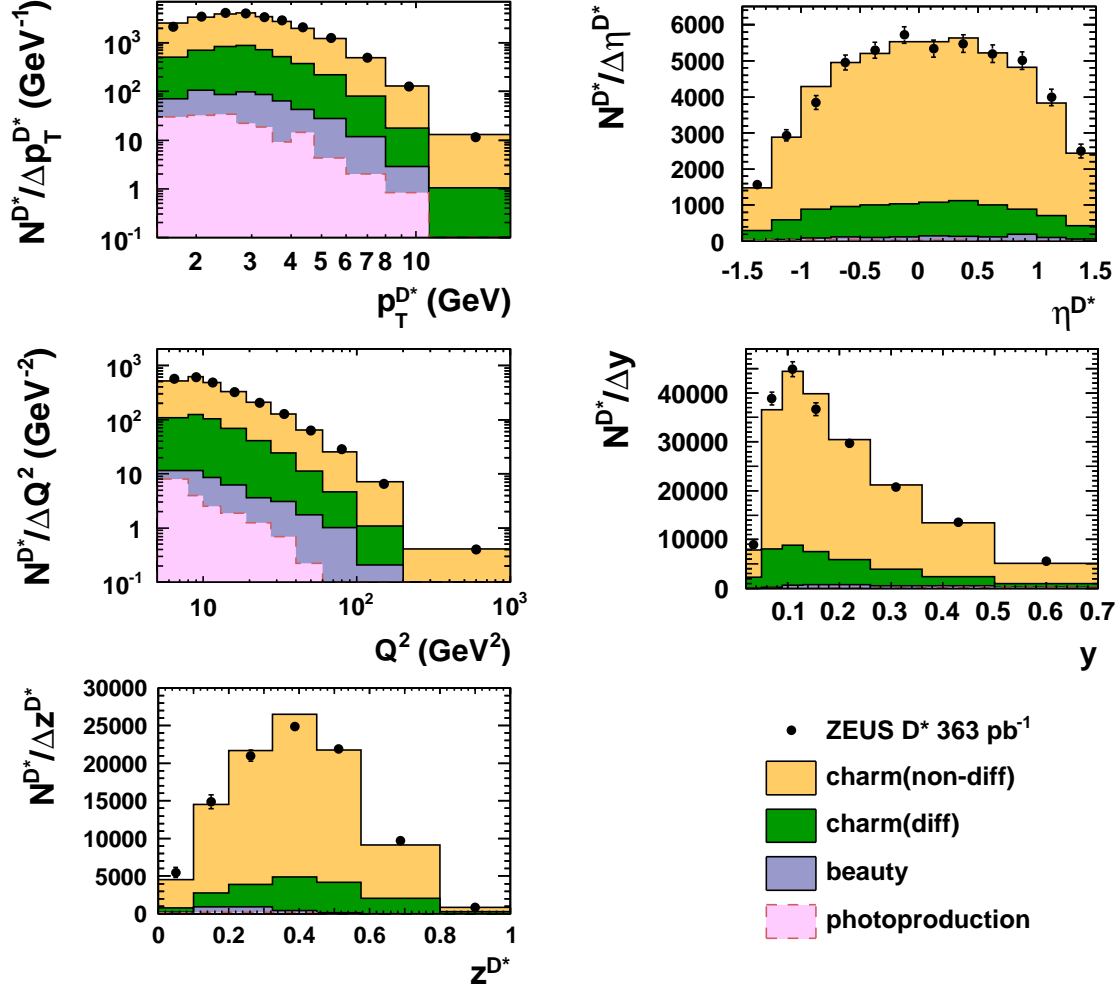
Figure 3: *Number of reconstructed $D^{*\pm}$ (filled circles), divided by bin size, as a function of $p_T^{D^*}$, η^{D^*}, Q^2, y and z^{D^*}. Data are compared to a MC mixture containing non-diffractive and diffractive charm production in DIS, beauty production, and charm photoproduction. The sum of the MC samples is normalised to the number of $D^{*\pm}$ in the data.*

26

ZEUS
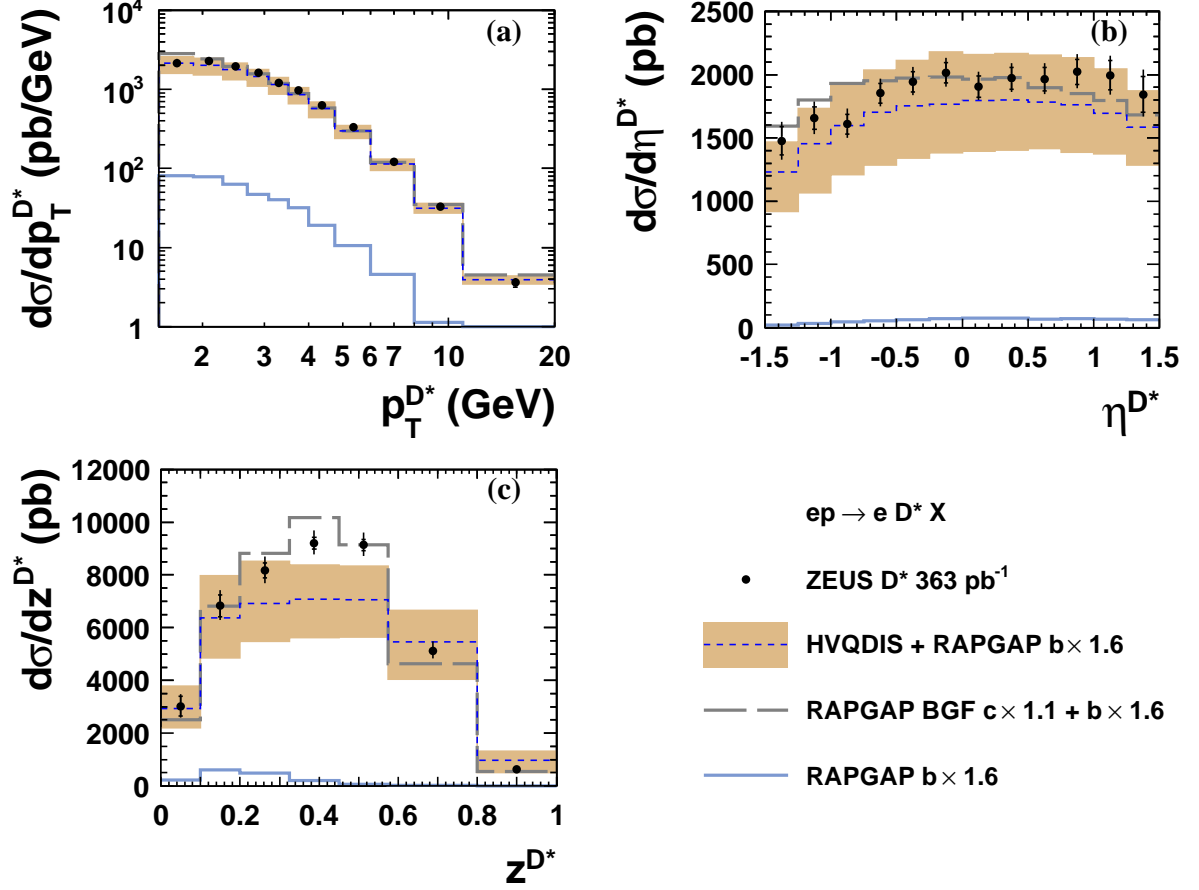
Figure 4: *Differential $D^{*\pm}$ cross sections as a function of (a) $p_T^{D^*}$, (b) η^{D^*} and (c) z^{D^*} (filled circles). The error bars show the statistical and systematic uncertainties added in quadrature, the inner bars show the statistical uncertainties alone. Also shown are NLO QCD predictions calculated using HVQDIS (dashed line and shaded area for the uncertainties) and RAPGAP MC prediction for charm creation via boson-gluon fusion (long-dashed line). The contribution from b-quark decays, calculated with the RAPGAP MC (continuous line), is included in the predictions. The MC cross sections for charm (beauty) are scaled by 1.1 (1.6) as described in the text.*

ZEUS
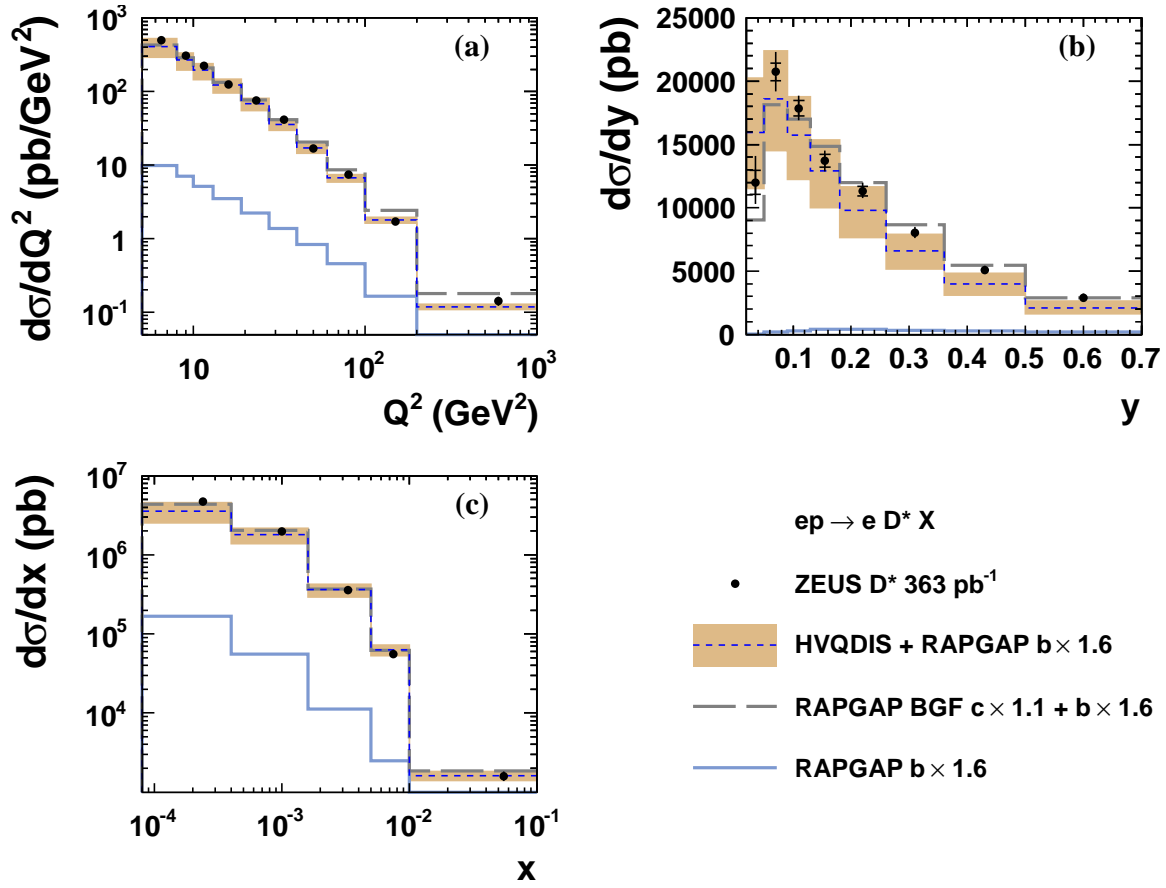
Figure 5: *Differential $D^{*\pm}$ cross sections as a function of (a) Q^2, (b) y and (c) x. Other details as in Fig. 4.*

ZEUS
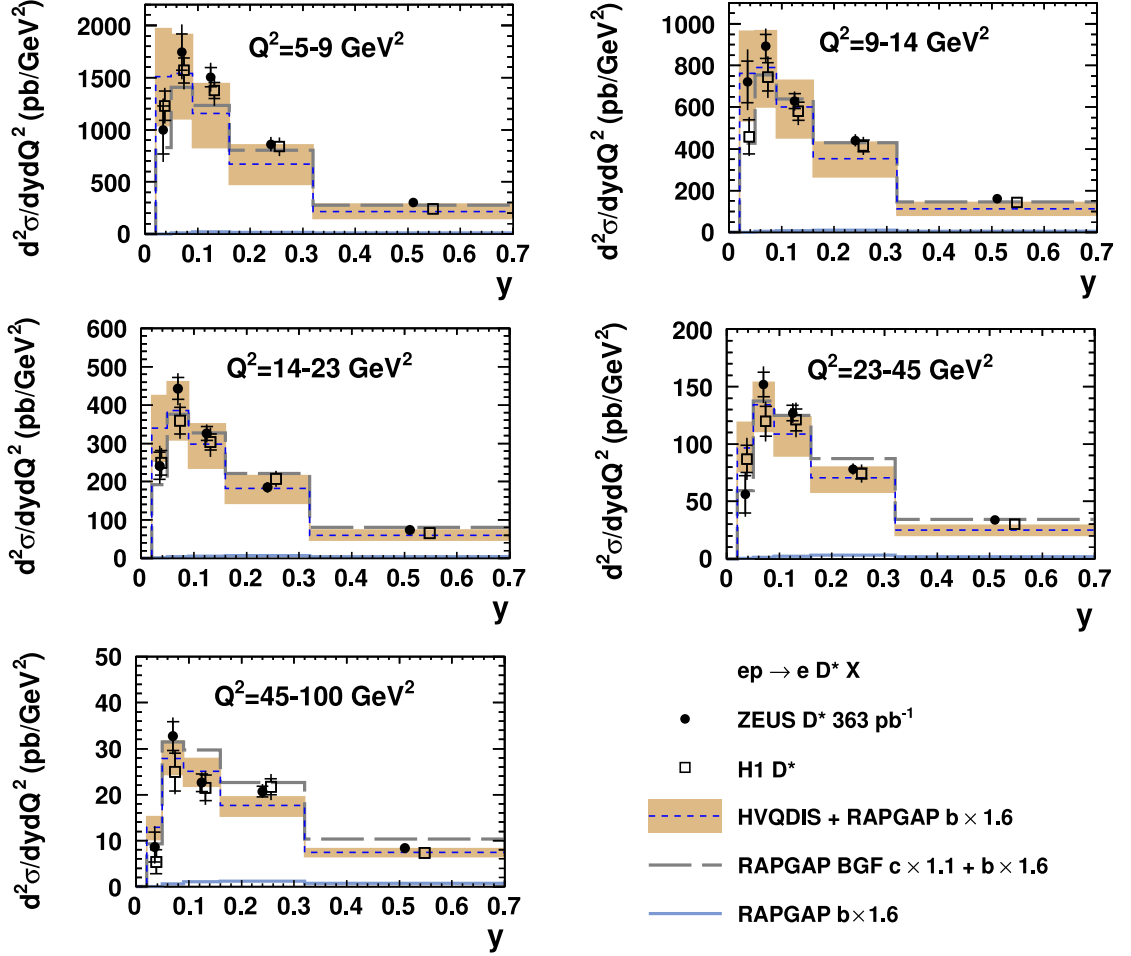
Figure 6: *Double-differential $D^{*\pm}$ cross sections as a function of Q^2 and y for $5 < Q^2 < 100 \ GeV^2$ (filled circles). The measurements from the H1 collaboration (empty squares) are also shown [17]. Other details as in Fig. 4.*
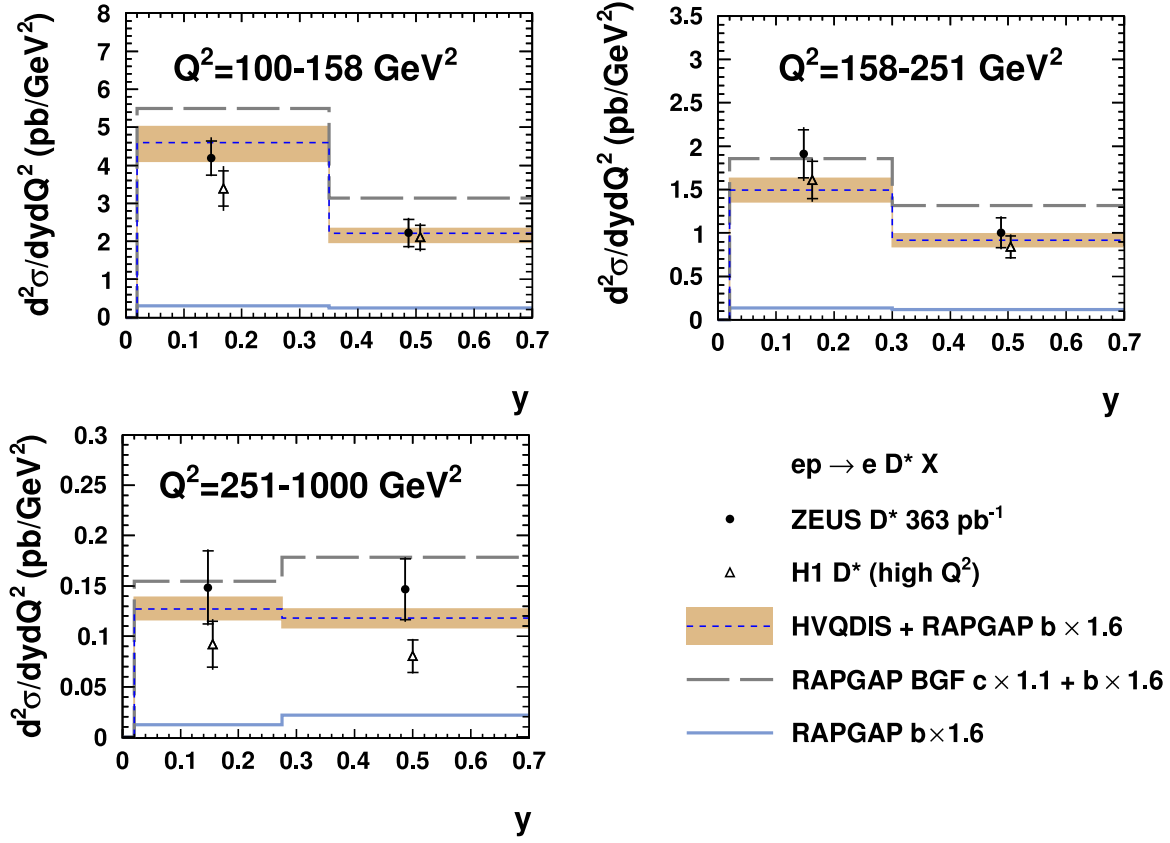
29

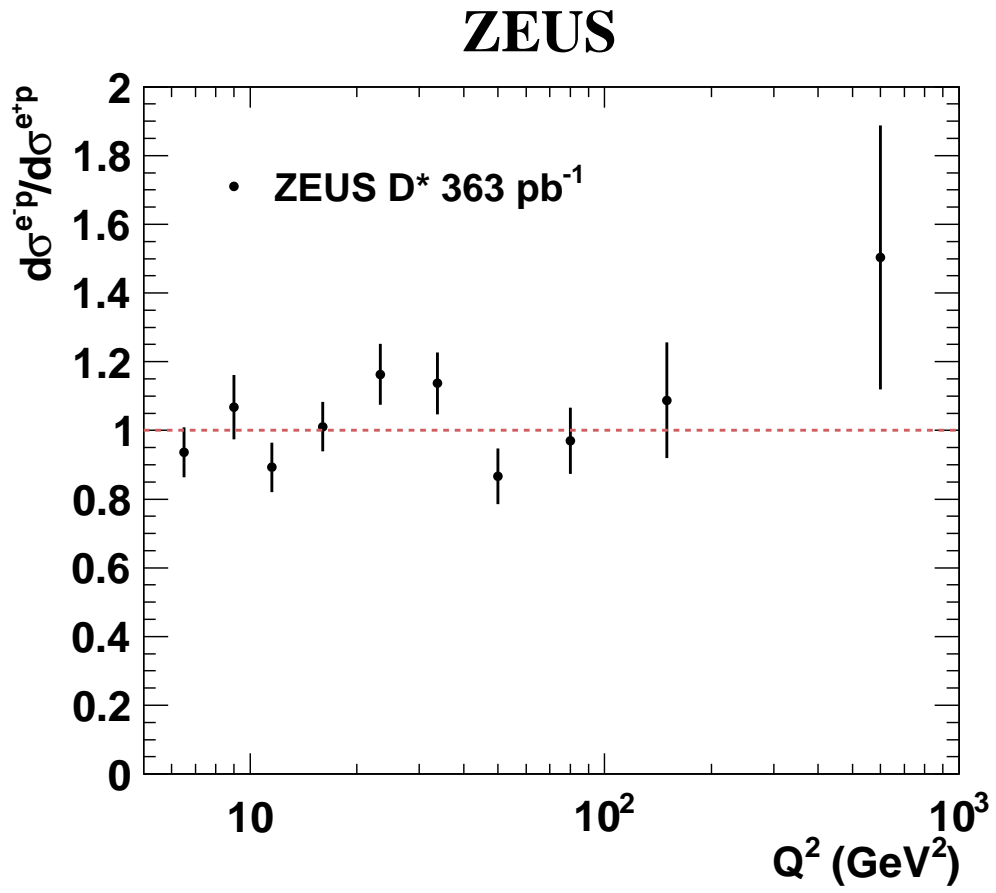**Figure 7:** *Double-differential $D^{*\pm}$ cross sections as a function of Q^2 and y for $100 < Q^2 < 1000$ GeV^2 (filled circles). The measurements from the H1 collaboration (empty triangles) are also shown [16]. Other details as in Fig. 4.*

Figure 8: *Ratio of e^-p to e^+p visible $D^{*\pm}$ cross sections as a function of Q^2. Only statistical uncertainties are shown. Bin boundaries are as in Table 4.*
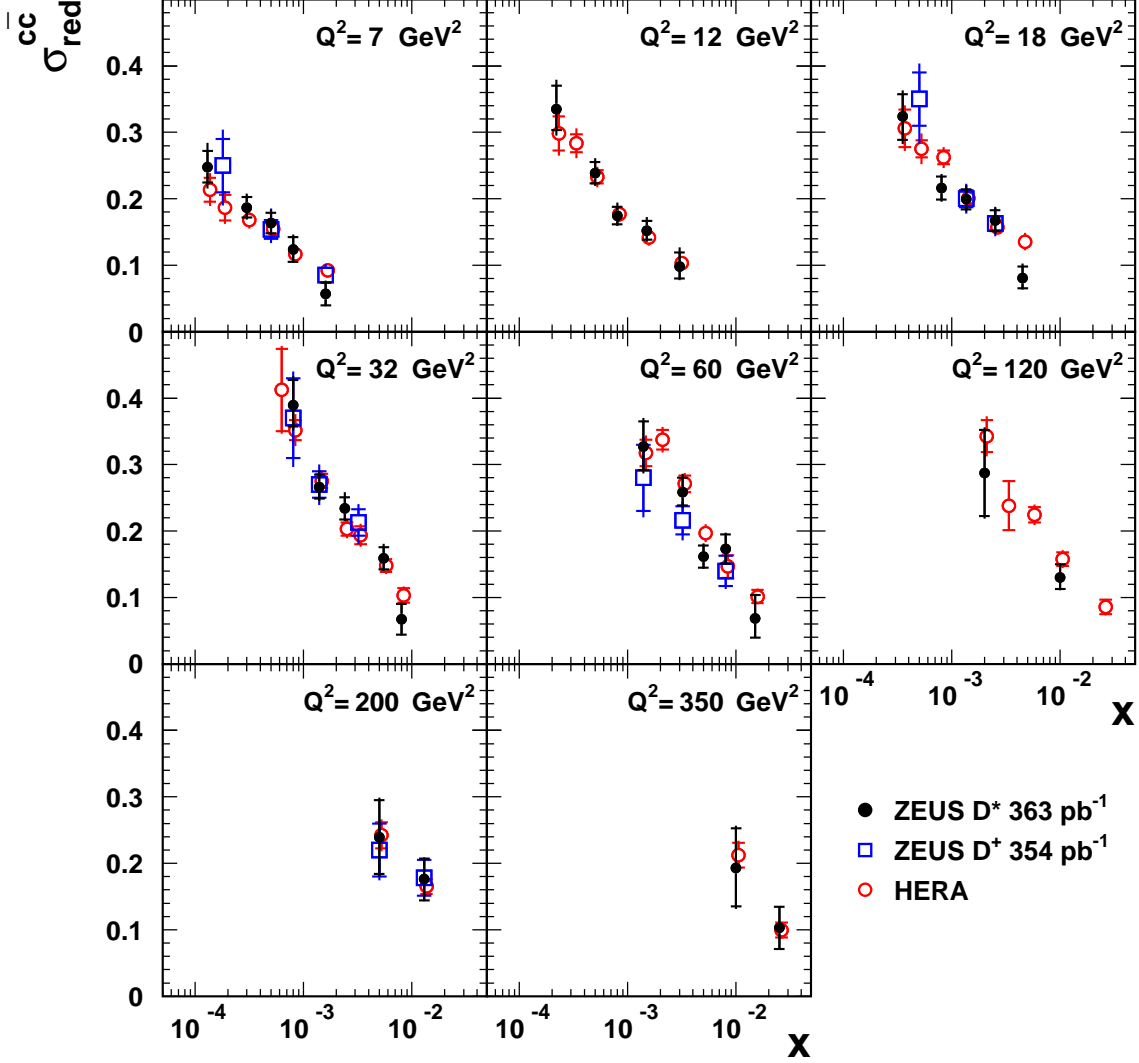
ZEUS

Figure 9: *Reduced charm cross sections from $D^{*\pm}$ (filled circles) compared to the ZEUS D^+ measurement [9] (empty squares) and the combination of previous HERA results [5] (empty circles). The outer error bars include experimental and theoretical uncertainties added in quadrature. The inner error bars in the ZEUS D^* and D^+ measurements show the experimental uncertainties. The inner error bars of the combined HERA data represent the uncorrelated part of the uncertainty.*
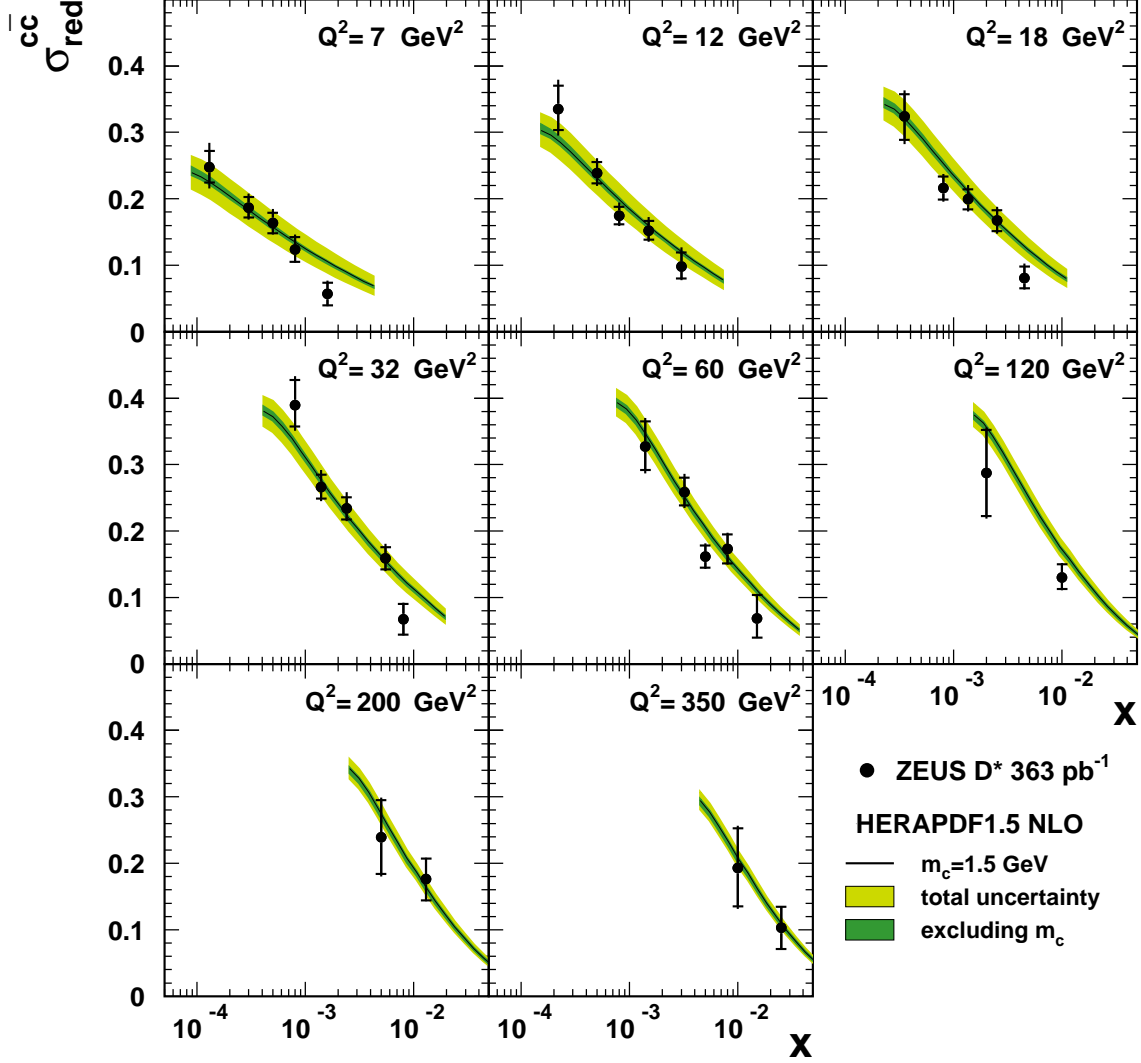
32

Figure 10: *Reduced charm cross sections (filled circles) compared to a GM-VFNS calculation based on HERAPDF1.5 parton densities. The inner error bars show the experimental uncertainties and the outer error bars show the experimental and theoretical uncertainties added in quadrature. The outer bands on the HERAPDF1.5 predicition show the total uncertainty while the inner bands correspond to the sum in quadrature of all uncertainties excluding the charm-mass variation.*